

A STUDY OF ARRAY SNR AND COUPLING AS A FUNCTION OF THE INPUT
IMPEDANCE OF PREAMPLIFIER

A Thesis

by

BIJAY KAMLESHBHAI SHAH

Submitted to the Office of Graduate Studies of
Texas A&M University
in partial fulfillment of the requirements for the degree of

MASTER OF SCIENCE

December 2007

Major Subject: Biomedical Engineering

A STUDY OF ARRAY SNR AND COUPLING AS A FUNCTION OF THE INPUT
IMPEDANCE OF PREAMPLIFIER

A Thesis

by

BIJAY KAMLESHBHAI SHAH

Submitted to the Office of Graduate Studies of
Texas A&M University
in partial fulfillment of the requirements for the degree of

MASTER OF SCIENCE

Approved by:

Chair of Committee,
Committee Members,

Head of Department,

Steven M. Wright
Eddy B. Boskamp
Mary P. McDougall
Jim X. Ji
Gerard L. Cote

December 2007

Major Subject: Biomedical Engineering

ABSTRACT

A Study of Array SNR and Coupling as a Function of the Input Impedance of
Preamplifier. (December 2007)

Bijay Kamleshbhai Shah, B.E., Saurashtra University, India

Chair of Advisory Committee: Dr. Steven M. Wright

Much of the current research in magnetic resonance engineering focuses on reducing the acquisition time for obtaining an image while simultaneously maximizing the Signal to Noise ratio (SNR) of the image. It is known that improvement in imaging time or resolution is obtained at the cost of SNR. Therefore wherever possible, RF coil engineers design the coil in such a manner so as to maximize SNR for that coil design. In one such design consideration, most coil designers prefer placing low impedance pre-amplifiers near the coil. The further the pre-amplifiers are from the coil, the greater will be the signal loss due to transmission and higher will be its input impedance as perceived at the coil which would degrade inter-coil isolation. Owing to the current trend of using increasing number of receiver channels (32, 64 or 128) for parallel imaging, placing the preamplifiers near the coil would greatly complicate the coil construction.

The primary objective of this research was to find the relation between SNR and referred preamp impedance and whether preamps need to be placed on the coil, or if they can be placed outside the magnet at the end of a transmission line which would simplify the construction of large count array. In addition, SNR was studied as a function of coil design parameters - coil loading, array coil separation, and system frequency. Both theoretical and experimental methods were used to undertake this investigation. A popular electromagnetic modeling technique, finite difference time domain (FDTD), was

used to model SNR in arrays of two 3 inch loop coils at 3T and 1.5T. Results were also verified through bench measurement at 3T and 1.5T and by evaluating SNR. To verify the robustness of our results and to assess the possibility of using low cost standard 50 ohm preamps, we carried out additional bench measurements at 4.7T. Results demonstrated that preamplifier placement is critical at low field strength. At higher field strength, SNR degradation due to preamplifier placement was less owing to heavier coil loading.

DEDICATION

To my loving family,
and
In memory of my loving aunt,
Asha Jayesh Desai

ACKNOWLEDGEMENTS

I would like to express my sincere appreciation for my advisor Dr. Steven Wright for his invaluable guidance and support throughout my graduate studies and for giving me an opportunity to work with him. Dr. Wright, it was a great learning experience working with you. I am thankful to you for keeping trust in me. I take this opportunity to wish you a great success in your research endeavors.

I am very thankful to Dr. Eddy Boskamp for being my advisor at GE Healthcare. Eddy, I will never forget your kindness to me – driving all the way to Milwaukee airport to pick me up, giving me rides to GE during initial days, welcome and farewell lunch.

I thank Dr. McDougall and Dr. Ji for their guidance and motivation. I am very grateful to my colleagues Naresh, Feng Ke, Vishal, John, Chieh Wei and James for sharing their knowledge and helping me out in my research. I also thank Scott Lindsay and LeRoy Blawat for useful discussions on RF coil design.

Mom and Dad, no words can best describe your love and caring for me. I am blessed to have you as my parents. I will always be indebted to you for making me what I am. Grandparents, you have taught me lessons that will help me in every step of my life. Thanks to my elder brothers, Jay and Sujay, for encouraging me and motivating me to excel in my academics. Thanks also to my sister-in-laws, Niki and Megha, for their moral support. Thanks to my niece Keya for her wonderful smile that makes my day.

I thank my friend, Suhani, for being a good companion during these years. To all my friends, I thank you all for being there for me and helping me every time when I needed it. Finally, I thank God for His blessings.

TABLE OF CONTENTS

	Page
ABSTRACT	iii
DEDICATION	v
ACKNOWLEDGEMENTS	vi
TABLE OF CONTENTS	vii
LIST OF FIGURES	ix
LIST OF TABLES	xii
CHAPTER	
I INTRODUCTION	1
A. Magnetic Resonance Imaging	1
B. Development of MRI and Parallel Imaging	2
C. Thesis Objective	4
1. Background	4
2. Problem Statement and Motivation	5
D. Outline of Thesis	6
II BACKGROUND	8
A. Principle of MRI	8
B. MRI Scanner	10
1. Main Magnet	10
2. Gradient System	10
3. Radiofrequency System	11
4. Computer	11
C. Transmit Coil	11
1. Homogeneity	11
2. RF Shield	12
3. Matching and Tuning	12
4. Decoupling	12
D. Receive Coil	13
1. SNR	13
2. Coupling in Coil Arrays	15
3. Receive Decoupling	17
4. Transmit Decoupling	19

CHAPTER	Page
5. Noise Matching of Preamplifier.....	20
6. Baluns and Cable Traps	20
III METHODS	22
A. Finite Difference Time Domain Modeling	22
1. Preliminary Simulations: Matching and Tuning.....	24
2. Simulations for SNR Modeling	28
3. SNR Estimation	32
B. Bench Measurements at 3T and 1.5T	34
1. Experimental Setup.....	34
2. SNR Estimation	36
C. Bench Measurements at 4.7T.....	37
IV RESULTS AND DISCUSSIONS.....	43
A. Finite Difference Time Domain Modeling	43
B. Bench Measurement.....	49
C. Other Results.....	52
D. Bench Measurement at 4.7T	54
V THESIS CONTRIBUTION	56
A. Procedure for Determining the Type and Placement of Preamplifier.....	56
1. Finding Coil to Phantom Distance for Maximizing SNR.....	57
2. Finding Distance between Two Next Nearest Elements in Coil Array	58
3. Method A – Obtaining Equivalent Two Port T-Network	59
4. Method B – Using Two Flux Probes to Measure Currents in Two Coils.....	61
B. Metrics for Decision Making.....	62
C. Decisions for 4.7T Experiment.....	63
VI CONCLUSION AND FUTURE WORK	65
REFERENCES	66
APPENDIX A.....	71
APPENDIX B	77
VITA.....	80

LIST OF FIGURES

FIGURE	Page
1	Use of low impedance preamplifiers for decoupling..... 5
2	Phenomenon of Nuclear Magnetic Resonance. In absence of external magnetic field, nuclear spins are aligned in random direction (a). In presence of external magnetic field, B_0 , more spins align parallel to the main magnetic field and produce longitudinal magnetization M_z (b). Application of an RF pulse (c) tips the magnetization vector to xy plane..... 9
3	Equivalent circuit of coil to understand various loss mechanisms when loaded with a patient..... 14
4	Coupling between two coils. Second coil is terminated with preamplifier of input impedance R_P at its output ¹⁹ 16
5	Geometric decoupling..... 17
6	Use of matching network in conjunction with low input impedance preamplifier for decoupling..... 18
7	FDTD model consisting of two coil array and tissue block..... 23
8	FDTD preliminary simulation to find random resonant frequency with known capacitance (a) Circuit diagram (b) Result: Impedance versus frequency plot..... 24
9	Preliminary simulation to find series resistance of the coil (a) Circuit diagram (b) Result: Impedance versus frequency plot – Series resistance (R_s) = 6.6Ω 26
10	Simulation to verify matching and tuning of the coil (a) Circuit diagram (b) Result: S_{11} versus frequency plot..... 27
11	Graphical model consisting of two coils loaded with tissue block. Experimental variables are system frequency f , inter coil distance d , coil to phantom distance D and preamplifier input impedance R 28
12	Circuit diagram for FDTD simulations at 3T ($f = 128.752\text{MHz}$)..... 30
13	Circuit diagram for FDTD simulations at 1.5T ($f = 63.8\text{MHz}$)..... 31
14	Typical FDTD result: Snapshot of B_1 field magnitude in plane perpendicular to plane of coil..... 33
15	Bench experiment: Actual setup..... 34

FIGURE	Page
16	Bench experiment: Graphical setup 35
17	3" Loop coil for experiments at 4.7T 37
18	Experimental setup for bench measurements at 4.7T 38
19	Experimental cases for coil 2 termination 40
20	(a) Low input impedance preamplifier (b) Test results: Input impedance = $(3.05 - j0.1)\Omega$; Gain 27.32dB (c) Standard 50 Ω preamplifier (d) Test results: Input impedance = $(52.42 - j7.3)\Omega$; Gain = 23.89dB 41
21	Schematic diagrams: Preamplifier placement a) Preamplifier placed on the coil b) Preamplifier placed at the end of 2λ coaxial cable 42
22	FDTD simulation results: SNR vs. distance from center of coil 1 along its axis [mm] 43
23	FDTD simulation results: SNR drop in dB vs. distance from center of coil 1 along its axis [mm] 44
24	FDTD results: SNR drop in dB vs. coil separation for different combinations of B_0 , R and D 45
25	B_1 field profile as a function of preamplifier input impedance R and phantom distance D at 3T for inter-coil distance $d=15\text{mm}$ 46
26	B_1 field profile as a function of preamplifier input impedance R and phantom distance D at 1.5T for inter-coil distance $d=15\text{mm}$ 47
27	Comparison of B , B_1^+ and B_1^- field profile for the case $B_0 = 3\text{T}$, $D = 24\text{mm}$, $d=15\text{mm}$ 48
28	Bench measurement results: S_{11} in dB vs. coil separation for different combinations of B_0 , R and D 49
29	Bench measurement results: S_{21} in dB vs. coil separation for different combinations of B_0 , R and D 50
30	Bench measurement results: SNR drop in dB vs. coil separation for different combinations of B_0 , R and D 51
31	ADS modeling results: SNR drop in dB vs. coil separation for different combinations of B_0 , R and D 52
32	Imaging experiment result: SNR drop in dB vs. coil separation for different combinations of B_0 , R and D 53

FIGURE	Page
33	Experiment A results: Current ratio I_2/I_1 vs. intercoil distance 54
34	Experiment B results: Current ratio I_2/I_1 vs. inter coil distance..... 55
35	Finding coil to phantom distance for maximizing SNR 57
36	Finding distance between two next nearest elements in the array 59
37	Surface coil with preamplifier decoupling network disconnected..... 60
38	Model of two coil represented as two port T-network with Z parameters..... 60
39	Determining current ratio using two flux probes..... 61
B1	S_{11} plot for experiment A at 4.7T 77
B2	S_{11} plot for experiment B at 4.7T 77
B3	S_{21} plot for experiment A at 4.7T 78
B4	S_{21} plot for experiment B at 4.7T 78
B5	S_{31} plot for experiment A at 4.7T 79
B6	S_{31} plot for experiment B at 4.7T 79

LIST OF TABLES

TABLE		Page
1	Experimental parameters for FDTD simulations and their values.....	29
2	Component values for FDTD modeling at 3T	30
3	Component values for FDTD modeling at 1.5T	31
4	Resistance and Q of the coil obtained using FDTD.....	35
5	Birdcage coil specification.....	39
6	Demonstration of selection of preamp configuration for two cases	63
7	Summary of recommended preamp configuration at 4.7T	64

CHAPTER I

INTRODUCTION

A. Magnetic Resonance Imaging

Magnetic Resonance Imaging (MRI) has become one of the most important imaging modality available for medical diagnosis and treatment planning. MRI is a non invasive and relatively safe imaging technique as compared to other imaging techniques like X-rays, Computer Tomography (CT) or Positron Emission Tomography (PET) which makes use of harmful ionizing radiations. While CT is limited to axial plane, MRI can capture images in axial, coronal as well as sagittal plane without moving the patient. In addition to anatomical information, MRI images also convey useful information regarding organ function and metabolic activities.

Since its inception in 1972, MRI has undergone rapid development both in terms of technology and clinical applications, because of the richness of the information available, and the unparalleled soft tissue contrast it provides. MRI has become preferred method for examination of brain and spinal cord with indications including suspected tumors, slipped disks, multiple sclerosis and degenerative diseases. It is widely applied for orthopaedics and musculoskeletal imaging. Specialized MRI techniques like MR Angiography (MRA), diffusion tensor imaging, functional MRI (fMRI) has greatly lead to the popularity of MRI¹⁻³.

The journal model is Concepts in Magnetic Resonance Part B: Magnetic Resonance Engineering.

B. Development of MRI and Parallel Imaging

The phenomenon of nuclear magnetic resonance (NMR) was discovered separately by Felix Bloch⁴ and Edward Purcell in 1946⁵. During early 1970s, Paul Lauterber⁶, Ray Damadian⁷ and Peter Mansfield⁸ independently pioneered the use of NMR for in-vivo imaging. This signaled the birth of MRI, which has evolved as an important imaging tool thereafter.

Earlier capabilities of MRI as an imaging tool were severely limited by the lengthy scan time needed to acquire an image. In addition, the images suffered from poor Signal to Noise Ratio (SNR). Developments in gradient capabilities have enabled faster sampling of k-space data. Techniques such as FLASH⁹, EPI and Spiral imaging have significantly improved the acquisition time for obtaining an image.

Advancement in fast imaging techniques was limited by factors that relate to human safety. Factors such as high field strengths, high gradient duty cycle and rapid application of RF pulses which are desirable for fast imaging are in turn unfavorable to the limits of specific absorption rate (SAR), a measure of energy deposited in tissue¹⁰. In addition, rapid traversal of k-space using fast switching gradients also leads to peripheral nervous stimulation¹¹⁻¹⁴.

During late 1980s, researchers began to explore the use of surface coil for improving SNR. Initially, surface coils were used as switched coils allowing different coils or combination of coils to be used for different slices¹⁵⁻¹⁸. Roemer et. al. described a method of simultaneously acquiring and combining data from multiple independent receiver coils for obtaining images with high SNR of surface coils while maintaining the Field of View (FOV) of volume coil without increasing acquisition time¹⁹. He referred

his technique as “The NMR Phased Array” and differentiated his array from switched arrays.

Even before the introduction of the phased arrays, the capability of multiple receiver coils in reducing acquisition time was being explored by several researchers²⁰⁻²⁴. Acquisition time in MRI is a function of the rate at which simultaneous and independent views of the object can be obtained where each view corresponds to each phase encoding step. By using the additional and independent views provided by the elements of surface coil array, one can reconstruct an image using reduced number of phase encode steps and thereby reduce the acquisition time²⁵. The above principle forms the basis for parallel imaging strategies. Practical implementations of parallel imaging were presented by Sodickson and Manning^{26,27}, and Pruessman, et al²⁸. Sodickson et al. proposed a method known as SMASH (SiMultaneous Acquisition of Spatial Harmonics) which is a k-space implementation of parallel imaging^{26,27}. Pruessman presented a general formulation and performance analysis of image domain SENSE (SENSitiving Encoding)²⁸. With these techniques, acceleration factors of two to four have become common in clinical settings while acceleration factors of 8 to 9 have become common in research sites. A new imaging technique called SEA imaging has been developed to explore the limits of acceleration in parallel imaging by completely eliminating phase encoding. In contrast to other parallel imaging techniques, this technique essentially acquires a “snapshot” in as little as a few hundred microseconds²⁹.

Parallel imaging has greatly revolutionized clinical applications of MRI. The increased speed and efficiency associated with parallel MRI may be employed for shortening long scans, improving spatial resolution, improving temporal resolution or

improving image quality. In addition to the body, cardiac and brain imaging applications, particularly promising areas of application for parallel imaging include functional MRI, contrast-enhanced MR Angiography, and diffusion tensor imaging. Other areas include spectroscopic imaging, musculoskeletal imaging pediatric imaging and dynamic/interactive MRI³⁰.

C. Thesis Objective

1. Background

Coil coupling has been considered undesirable in NMR phased arrays and parallel imaging. When two resonant loops that are tuned to same resonant frequency f_0 are placed near each other, the mutual inductance between coils causes the resonances to split. The splitting results in loss of sensitivity at the frequency f_0 ¹⁹. Further they resonate as a single structure and it can be difficult to match the impedance of each element simultaneously to the input impedance of receiver. When this match is non-optimal, the preamplifier noise figure can be seriously degraded, leading to an image with poor SNR.

The introduction of parallel MRI technique has led to renewed emphasis on removing coil coupling and maintaining coil isolation. Each coil in the array should have a sensitivity profile as distinct as possible in order to encode spatial information. When coils couple inductively, they become sensitive to the same regions of the sample, and it has been feared that coupled coils might contain less distinct spatial information than uncoupled coils, yielding lower quality parallel MR image reconstruction. Although there has been recent debate^{31,32} questioning the necessity of minimizing signal coupling to achieve optimal SNR and parallel imaging performance, 3D imaging still requires the coils be decoupled.

Several methods, as discussed in chapter II, have been developed to minimize the effects of coupling and mutual inductance. This research explores the method of using low input impedance preamplifier to decouple the coils. Low impedance preamplifiers are used to present a large impedance to current flow at the input of each coil¹⁹. As shown in Figure 1, if the input impedance of the preamplifier R_p is truly zero, the inductor forms a parallel resonant circuit with the capacitor and blocks the current from flowing (due to high impedance) in the surface coil even though the coil is receiving and faithfully transmitting NMR signal to preamplifier.

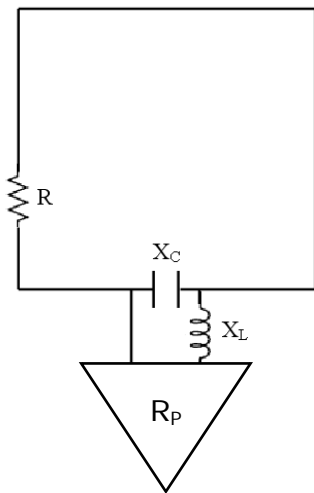


Figure 1 Use of low impedance preamplifiers for decoupling

2. Problem Statement and Motivation

Most manufacturers prefer placing the preamplifier close to the coil in order to have better coil isolation and better SNR³³. Owing to the fact that maximum theoretical acceleration is equal to the number of independent receiver channels, parallel imaging has led to the trend of using increasing number of receiver channel – 32, 64 or 128.

Constructing a coil with such a large number of receive chain itself is very challenging and complex. Placing the preamplifiers on the coils would further complicate the coil design. This complexity can be reduced to some extent if preamplifier can be located remotely.

This research aims at exploring the possibility of placing the preamplifiers at the end of $n\lambda/2$ transmission line that would bring the preamp outside the magnet. In addition, SNR was studied as a function of inter-coil distance, coil loading and system frequency.

50 Ω standard preamplifiers are readily available in the market and their use instead of low impedance preamp would greatly reduce the cost of large count coil arrays. Therefore, the possibility of using low cost 50 Ω standard preamplifier was also investigated.

Significance of this research can well be seen by understanding the applications of parallel imaging. Dynamic imaging would not have been realized without the advances in parallel imaging technology.

D. Outline of Thesis

Chapter I has given a brief introduction about MRI, the development of MRI and recent advancement in MRI – parallel imaging along with their application as diagnostic tool in medicine. To understand the purpose behind the use of low input impedance preamplifier, a short technical background regarding coil coupling and its role in reducing SNR was presented. Problem relating to decision regarding the preamplifier placement was introduced along with other objectives behind this research and its significance.

Chapter II gives an overview of the MRI principle and instrumentation. Primary coil design criteria, homogeneity for the transmit and SNR for receive, are described. Basic information relating to RF coil design is presented. Coupling theory between two receive coils is presented. Need and methods of decoupling between transmit and receive coil and between receive coils are described.

Chapter III describes two different methods, Finite Difference Time Domain (FDTD) and Bench measurement, for studying SNR in two coil array as a function of coil design parameters (i) input impedance of the preamplifier (ii) inter coil distance (iii) coil array to patient distance and (iv) static magnetic field strength. It also describes bench studies at 4.7T to assess coupling between two coils as a function of preamplifier input impedance and placement.

Chapter IV presents and discusses results of the above experiments. In addition, results of ADS modeling and imaging experiments for SNR studies are also presented.

Chapter V provides information regarding two methods for evaluating coupling between two coils. A metrics for making decision in regard to preamplifier type and placement is presented with examples.

Chapter VI summarizes the research and describes the future work in this direction.

CHAPTER II

BACKGROUND

A. Principle of MRI

Human body has plenty of hydrogen atoms in the form of fat and water. A hydrogen atom consists of a nucleus containing a single proton and a single electron orbiting around the nucleus. As a rotating mass (m), the proton has angular momentum while as a rotating mass with a positive electrical charge; it has magnetic moment (B) and behaves like a small magnet.

As shown in Figure 2, in absence of external magnetic field, the individual magnetic moment or spins are oriented in random direction resulting in net zero magnetic moment. When subject to external magnetic field, B_0 , the magnetic moments, or spins, align with the direction of the external field. The magnetic moments do not align with the external field but, like spinning tops, undergo precession. Precession of nuclei occurs at a characteristic speed that is proportional to the strength of applied magnetic field and is called Larmor frequency.

As the spins get aligned to the external magnetic field, longitudinal magnetization M_z starts building up in z-direction because the magnetic vectors representing the individual magnetic moments add together. Actually, the spins align parallel or anti-parallel to the magnetic field with parallel alignment being slightly preferred because it is more favorable energy state. Hence, under steady state condition, a slightly larger fraction aligns parallel to the main field than anti-parallel. It is this small difference that produces a measurable net magnetization vector that is detected in MRI.

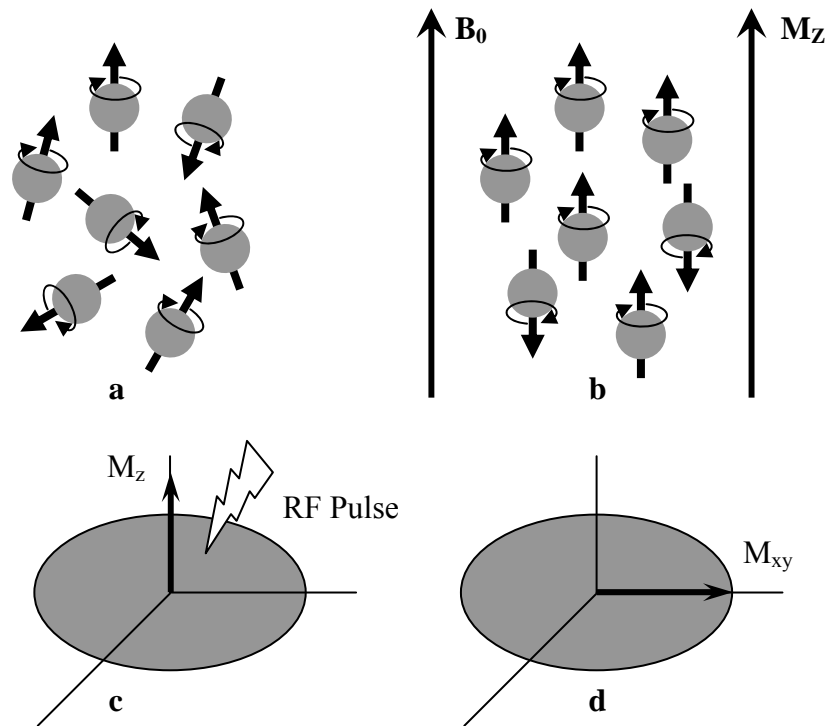


Figure 2 Phenomenon of Nuclear Magnetic Resonance. In absence of external magnetic field, nuclear spins are aligned in random direction (a). In presence of external magnetic field, B_0 , more spins align parallel to the main magnetic field and produce longitudinal magnetization M_z (b). Application of an RF pulse (c) tips the magnetization vector to xy plane

Energy can be introduced into such a stable spin system by applying an electromagnetic wave of frequency equal to larmor frequency. This required electromagnetic wave is generated by using RF coils. This energy results in the longitudinal magnetization being more and more tipped away from z -axis towards xy -plane perpendicular to the direction of the main magnetic field. If the applied RF pulse that is long enough and strong enough to tip the magnetization by exactly 90° is applied, the longitudinal magnetization is rotated into transverse plane. The resulting magnetization is now referred by M_{xy} or transverse magnetization. The magnetic moment vectors still precess about the z -axis and induce an alternating voltage of same

frequency as Larmor frequency in a receiver coil. This signal is collected and processed with computers to generate image³⁴.

Application of RF energy in presence of external magnetic field to resonate nuclear magnets is termed as nuclear magnetic resonance.

B. MRI Scanner

MRI scanner consists of several components as described below:

1. Main Magnet

A strong magnet is needed to generate the static magnetic field (B_0). The magnet should generate homogenous magnetic field in the region of interest. When the magnets are unable to provide homogenous magnetic field, shim coils are used to increase field homogeneity or uniformity. Current clinical magnets operate at 1.5T or 3T field strength while magnets in research site typically have high field strength – 4.7T or 9.4T. The NMR signal induced in the receive coil and therefore the SNR increases as the square of the Larmor frequency, in other words as the square of the static magnetic field strength B_0 ^{35,36}.

Initial magnets were either permanent magnets or resistive magnets. Currently, the static field B_0 is generated using superconducting magnets.

2. Gradient System

Magnetic field gradients are applied for slice selection and spatial encoding. Gradient system is made of three gradient coils, each with its own amplifier, to create a linear change in magnetic field as a function of distance (field gradient) along x-, y- and z- axes. Gradient performance is measured by three parameters:

Maximum gradient strength (mT/m)

Rise time – time to maximum gradient amplitude

Slew rate – maximum gradient amplitude/rise time.

3. Radiofrequency System

The RF system consists of the transmit and receive chain associated with the transmit and receive coils. These may be combined coils acting both transmitters and receivers such as the body coil which is integrated into the scanner. However for most applications, a body coil may be used as transmit coil while a separate multiple receive coils are used to detect the NMR signal to improve SNR.

4. Computer

The computers of MR system is used to control gradients and RF coils. They are also used to obtain the data, process it and obtain an image.

C. Transmit Coil

1. Homogeneity

The purpose of the transmit coil is to convert electrical energy into a highly homogenous RF magnetic field. This is mostly achieved by using a Birdcage coil resonator. Appropriate value capacitors are used to make the birdcage coil resonant at frequency of interest. The configuration of birdcage is dependant upon the placement of capacitors. Low pass birdcage coils have capacitors on the rungs, while high pass birdcages have them on the ring. Capacitor placement determines the E field pattern generated by the coil, which is important for reducing power deposition in tissue.

In order to generate perfect homogenous transverse field, amplitude of the rung currents in the birdcage should vary as a sine of the azimuthal angle. Since the coil cannot be

infinitely long, the field in z direction is not going to be as homogenous as compared to that in xy plane.

2. RF Shield

It is necessary to shield RF coils to prevent coupling with other structures in MR system. Body coils have huge stray fields and are likely to have severe interaction with the gradient coils and the cryostat. RF shield separates the transmit coil from the gradient coil environment, which is a lossy structure. However, it should also be transparent for the gradient fields, otherwise gradient eddy currents may be induced in the shield leading the shield heating and increase in rise time causing artifacts in the image. Gradient rise time is on the order of 0.1 ms that corresponds to 10kHz. To make the shield transparent to gradient pulses, it is cut at several locations and bridged with nF capacitors. The efficiency of an RF coil highly depends on the distance between the shield and the coil.

3. Matching and Tuning

For maximum power transfer, the input impedance of the coil has to match the output impedance of the power amplifier. Typically, this impedance is 50Ω and therefore the connection should also be made with 50Ω coaxial cables.

4. Decoupling

During the detection phase, the receive coils detect the NMR signal during which the transmit coil should be turned off. Both the coils operate at same frequency; therefore if the body coil is not turned off, energy would be transferred between the two coils. Further, body coil detects a much larger patient volume than the receive coil. So, noise associated with RF losses in that patient detected by body coil couples with the receive coil and destroys the SNR.

Body coil can be turned off by employing PIN diode network that forms a part of parallel resonator. The inductance is chosen such that the resonance frequency is same as that of imaging coil. When PIN diode is forward biased, the parallel circuit becomes resonant and will have high impedance at its insertion points, effectively opening up the circuit at that point. DC bias line needs to be decoupled from RF and should be routed such that it cannot generate B Field^{37,38}.

D. Receive Coil

1. SNR

Whereas the transmit coils are designed for achieving better field homogeneity, the primary design criteria for receive coil is to achieve highest SNR.

Following equation describes the relation between SNR and coil parameters – loaded Q (Q_L) and effective volume V_{eff} .

$$SNR \propto \sqrt{\frac{Q_L}{V_{eff}}} \quad \text{where} \quad \frac{1}{Q_L} = \frac{1}{Q_0} + \frac{1}{Q_{pat}} \quad V_{eff} = \int \frac{B_1^2}{B_{1(ROI)}^2} dV$$

In order to optimize SNR, the loaded Q_L should be at least a factor 5 smaller than unloaded Q_0 ; which means patient noise is dominant noise source, and coil losses are not significant.

The effective volume of the coil, V_{eff} , is the volume integral of magnetic energy in the entire volume normalized on that of the region of interest. It is different from the geometric volume. To optimize V_{eff} to achieve highest SNR, the coil has to fit the anatomy of interest and should not be made any larger than necessary. Ratio of effective volume and geometric volume is called filling factor. The effective volume depends on the size of the coil and size of the conductors, since areas near to the conductors contribute heavily to the volume integral.

Quality factor of the coil is determined by the series resistance, which is contributed by the coil losses R_C , dielectric losses R_D and eddy current losses R_{EC} . Figure 3 shows the various loss mechanism that affect Q of the coil when loaded with a patient.

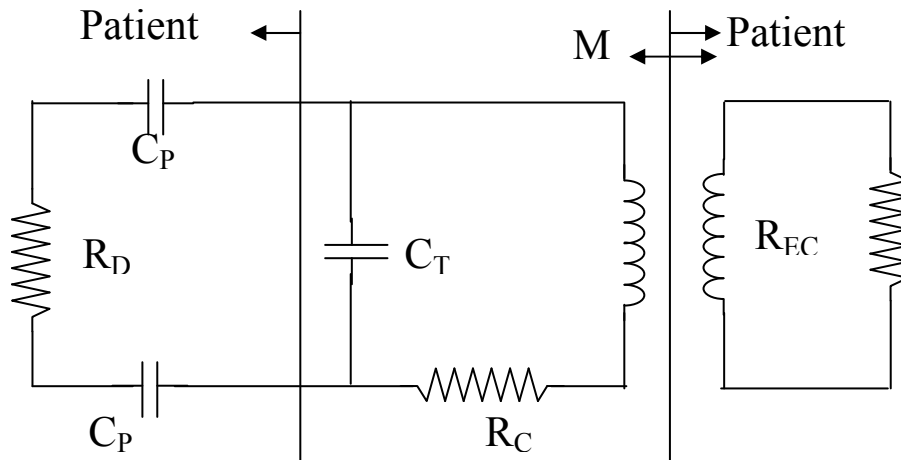


Figure 3 Equivalent circuit of coil to understand various loss mechanisms when loaded with a patient

Coil losses are associated with the conductivity of the conductor material and determine the Q of the empty coil. By using copper as a conductor and high Q ceramic capacitors, coil losses can be minimized. Coil losses are only a small fraction of the total losses once the coil is loaded with a patient, except at frequencies below 10MHz. At lower frequencies, conductor length and cross section area determines its resistance. At radio frequency, current density decays exponentially with depth into the conductor, with a decay constant δ which is called skin depth. Therefore at this frequency, the circumference and smoothness of the conductor matters. Sharp corners and bends in conductor will increase its resistance and also give rise to radiation losses.

The dielectric losses R_D are caused by parasitic capacitance C_P that forms between the coil and the skin of the patient. Dielectric losses can be minimized by using tuning capacitance C_T an order of magnitude higher than the parasitic capacitance and placing them away from the patient. This prevents flow of current via these parasitic capacitors and thereby minimizing losses and a frequency shift upon patient loading.

The eddy current losses are caused by interaction of RF magnetic field with the patient. Eddy currents are setup in tissue in response to changing magnetic fields according to Lenz's law. These eddy currents are the major loss mechanism at 1.5T and determine 95% of the total loss resistor. Since this is a mutual coupling, eddy current losses increases with the square of frequency. Therefore, at lower field strength, it is not the eddy current losses but the coil losses that are dominant factor which signifies the use of superconducting coils at lower frequency. Eddy current losses are inherent to the processes in MRI and cannot be overcome by smart coil design^{37,38}.

2. Coupling in Coil Arrays

In a multi-coil array, each coil experiences both thermal noise and noise coupled from the neighboring coil. Coupling can be considered as transfer of signal from one coil to another coil because of mutual inductance. The noise produced by each coil is the sum of the thermal noise and the coupled noise from neighboring coils³⁹. To understand coupling between surface coils, consider the figure shown below

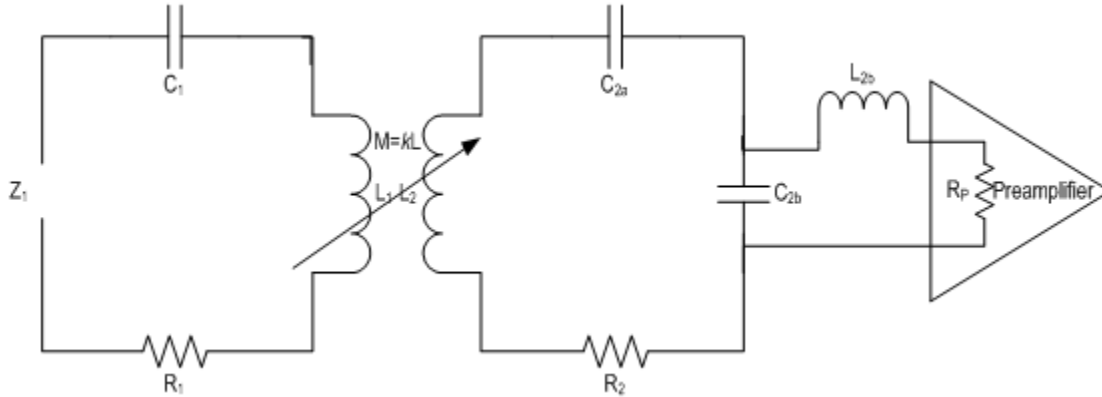


Figure 4 Coupling between two coils. Second coil is terminated with preamplifier of input impedance R_P at its output¹⁹

Suppose that coils in Figure 4 are tuned to same resonant frequency. In absence of second coil, the impedance viewed at first coil Z_1 would be R_1 since the capacitive and inductive reactance cancels each other while the coil is resonating. Here R_1 is the sum of total noise resistance R_C (coil losses), R_D (dielectric losses) and R_{EC} (eddy current losses). With the second coil present and terminated with preamplifier of input impedance R_P , the impedance as viewed from the terminals of the first coil is given by

$$Z_1 = R_1 + \frac{\omega^2 L^2 k^2}{R_1 + \left(\frac{X_2^2}{R_P} \right)} \text{ where } X_2 = X_{L_{2b}} = X_{C_{2b}}$$

The second term in the above equation represents the impedance associated with noise power coupled between two coils. Here if either the mutual inductance coupling constant k is made zero or the input impedance of the preamplifier is made zero, the term approaches zero and the resultant noise resistance is R_1 , that of a single isolated coil.

The above equation also dictates the two ways to minimize the effects of coupling: reduce the mutual inductance, or reduce the input impedance of the preamplifier and thereby reduce the coil currents^{19,40}.

3. Receive Decoupling

In case of multi coil array, individual coils need to be decoupled from each other during receive phase to sustain the SNR of the coils and to avoid image artifacts caused by coupling. Several methods have been proposed to remove the effects of mutual inductance. One method involves building capacitive or inductive networks between coils that would cancel exactly the mutual inductance or capacitance between them⁴¹⁻⁴³.

Alternatively, adjacent coils can be overlapped as shown in Figure 5 to force the mutual inductance to zero. This method cannot be applied for an array with more than three elements. Further the overlap is very sensitive and load dependent.

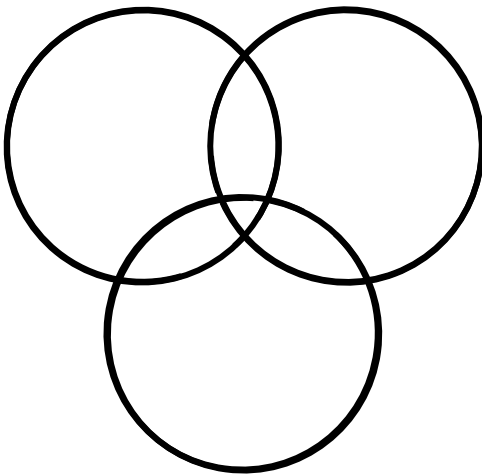


Figure 5 Geometric decoupling

For orthogonal coils, such as properly aligned planar pair loop combination, mutual impedance Z_{12} is zero. There is no need for using isolation preamplifiers as the mutual resistance and mutual reactance are zero and the effects of coupling are eliminated. Further there is negligible noise correlation since mutual resistance is zero.

As described earlier, Roemer introduced method of using low input impedance preamplifier that presents high impedance at the coil to minimize coil currents and thereby decouple the coils. Appropriate matching networks as shown in Figure 6 may be employed that convert the low impedance of preamplifier to high impedance at the coil and in reverse direction convert coil impedance to standard 50Ω at the preamplifier side for ensuring optimal noise performance of the preamplifier^{19,40,44}.

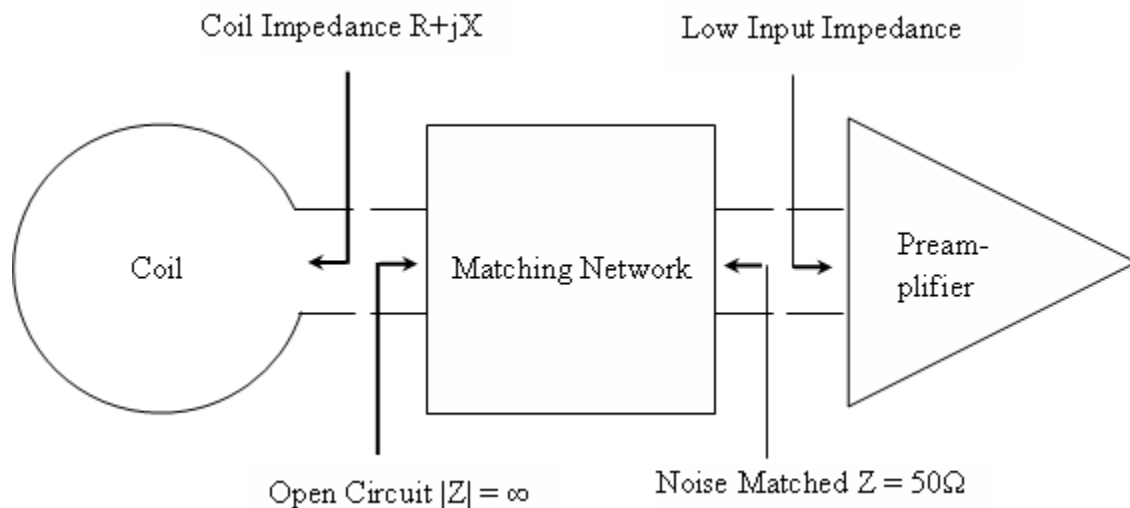


Figure 6 Use of matching network in conjunction with low input impedance preamplifier for decoupling

In practice, interaction with nearby surface coils is eliminated by overlapping adjacent coils to give zero mutual inductance and by attaching low impedance preamplifiers to all coils thereby eliminating interaction among next nearest and more distant neighbors.

4. Transmit Decoupling

Each coil in a multi coil array is a surface coil designed to receive the signal from the nuclear spins. Each of these receive coils should be turned off and decoupled from the transmit coil usually a body coil during RF excitation pulses. Otherwise a large current will be induced in the receive coil, destroying the transmit uniformity, damaging the preamplifiers and other coil electronics and exceeding SAR limits. This can be achieved by creating a high impedance at the coil and thereby minimizing the currents on the coil induced by transmit field. There are two approaches for achieving this: passive detuning and active detuning. Both approaches make use of PIN diodes which when forward biased cause parallel inductor-capacitor network to resonate leading to high impedance across the parallel circuit.

Passive Detuning

Simplest method is passive detuning which relies on the ability of transmit field to forward bias a pair of crossed high speed diodes. In most cases, these diodes act as a switch connect a parallel resonant trap to the coil thus opening the coil. If the transmit field is not strong enough, the diodes will not be fully switched on and interaction between transmit and receive coil will still persist. The method is, therefore, not highly reliable and therefore is used as a redundant safety decoupling mechanism to active detuning.

Active Detuning

Active detuning is more reliable but requires DC bias voltage to operate PIN diodes. The logic signal required to switch the coil between transmit and receive state is supplied by RF power amplifier's unblank signal^{32,37,38}.

5. Noise Matching of Preamplifier

Thermal noise is generated by all components including preamplifiers. This noise is characterized by the noise figure or noise factor F . Noise figure is the ratio of output to input Signal to Noise Ratio (SNR). The first stage of amplification (ie preamplifier) in receive chain is the most critical since the noise figure, F , of the receive chain is calculated from individual noise figures F_i and gains G_i as

$$F = F_1 + \frac{F_2 - 1}{G_1} + \frac{F_3 - 1}{G_1 G_2} + \frac{F_4 - 1}{G_1 G_2 G_3} + \dots$$

This equation implies that any noise circuit placed before the preamplifier will have great impact on the achievable noise performance. Therefore, great care should be taken in designing matching network between the coil and the preamplifier. Low loss components such as air wound inductors should be used while the use of cables between the coil and the preamplifier should be eliminated^{32,37,38}

6. Baluns and Cable Traps

Coils do not have well defined ground. This is especially true for receive coils. The only well defined ground is at the end of cable where it is connected to the system. Parasitic capacitances between the coil, shield and cable, together with self inductance of cable give rise to cable resonances. High voltages may occur at the coil side of the cable shield, setting up a standing wave in the coax shield. One method to prevent this is to have coil drive points as symmetric as possible such that virtual ground points are created

in the coil where cable shield can be attached. Further, “Balun” can be used in series with the cable to create high impedance for shield currents on the outside of the cable, but letting the signal through unaffected. To make a balun, one can loop a cable into several turns and then resonate out the associated shield inductance with a capacitor, thus creating a parallel tank circuit^{37,38}.

CHAPTER III

METHODS

Signal to noise ratio was studied in an array consisting of two coils loaded with a phantom having properties similar to the body tissues at 3T and 1.5T. Parameters were: the input impedance of the preamplifier, distance to the load, distance between the coil elements and frequency. The study was carried out using Finite Difference Time Domain Modeling technique. The results were verified using bench measurements.

Bench measurements were carried out at 4.7T to study coupling between two coils in order to determine effectiveness of decoupling preamplifiers as a function of its input impedance and placement. The above methods are described in this chapter.

A. Finite Difference Time Domain Modeling

Finite difference time domain is a popular electromagnetic modeling technique to model engineering problems dealing with electromagnetic wave interactions with material structures. It is easy to understand and easy to implement in software.

In order to carry out theoretical modeling in FDTD, first a computational domain is established. Computational domain is simply the physical region over which simulation will be performed and E and H fields will be calculated. Computational domain is then divided into cell, and material property of each cell in the computational domain is specified. Typically, the material is free space (air), metal or dielectric. Any material can be used as long as the permeability, permittivity and conductivity are specified. Once the computational domain and materials are established, the source is specified. The source can be an impinging plane wave, a current on a wire, or an applied electric field depending upon the problem. Since the computational domain must be finite to permit its

residence in the computer memory, appropriate boundary condition should be used to simulate for infinite unbounded computational domain⁴⁵.

A model was constructed in Remcom's XFDTD software as shown in Figure 7. Two 76.2mm diameter loop shaped coil made from 5.1mm wide copper strip loaded with a muscle tissue block of dimension 260 x 90 x 160 mm was created. The muscle tissue block was modeled with conductivity of 0.7 S/m and a relative permittivity of 80. Cell dimensions were chosen as 1.6 x 1.6 x 1.6 mm - small enough to represent the smallest feature in the model and smaller than one tenth of the smallest wavelength to be used for excitation. LIAO absorbing boundary conditions were selected for all the simulation to reduce the simulation time.

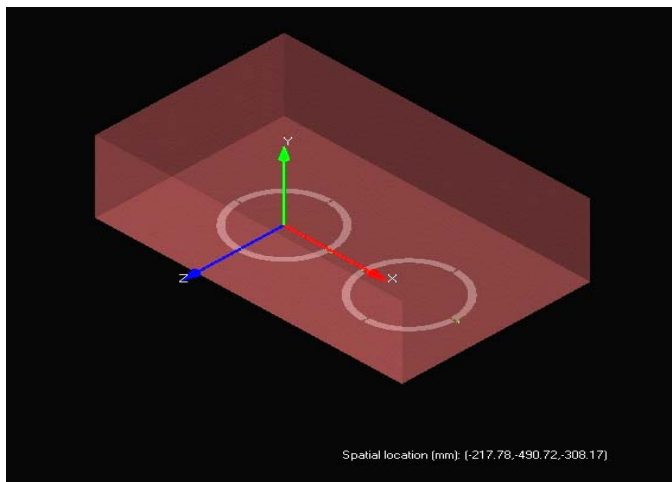


Figure 7 FDTD model consisting of two coil array and tissue block

1. Preliminary Simulations: Matching and Tuning

Preliminary simulations were done to tune the coil at desired frequency f (127.7MHz and 63.8MHz) corresponding to 3T and 1.5T and match it to 50Ω for different cases of tissue to coil distance (D). The method of finding tuning and matching capacitors and blocking inductor for a typical case of 3T with coil to tissue distance $D = 8\text{mm}$ is described here.

Initially, coil 1 was tuned at random frequency using a parallel resonating circuit as shown in Figure 8(a) by a broadband excitation; coil 2 was left open and unexcited. Result of this simulation shown in Figure 8(b) showed that the circuit resonated at 138.656 MHz.

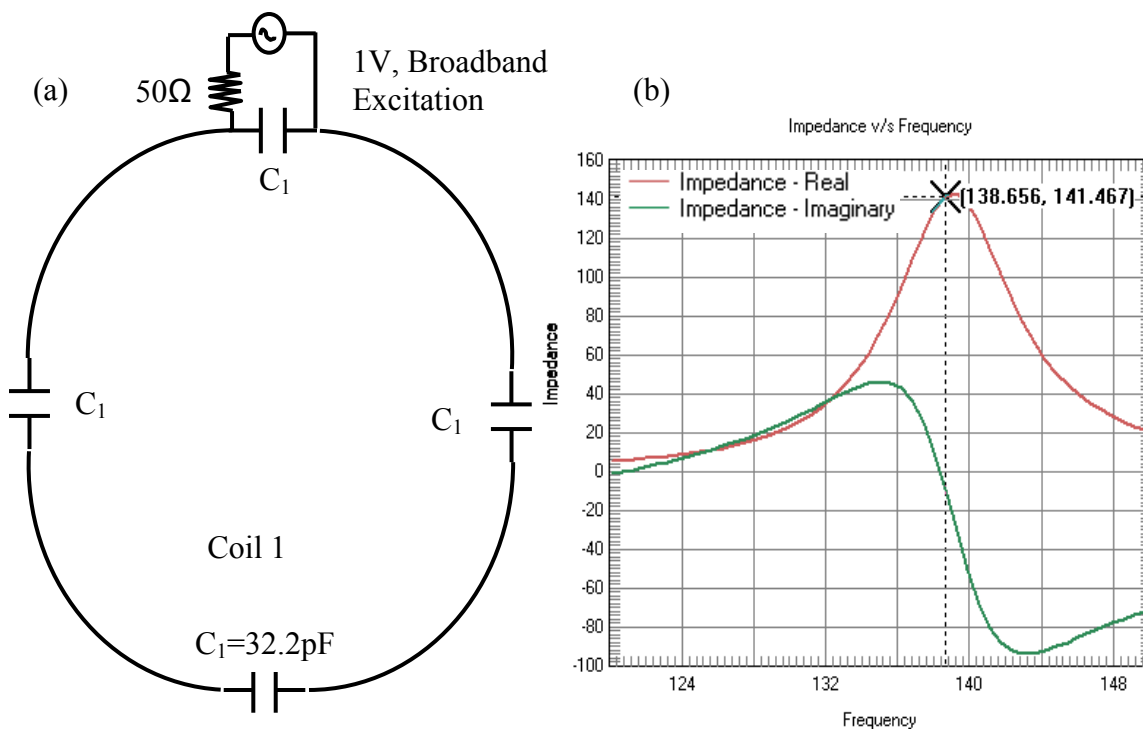


Figure 8 FDTD preliminary simulation to find random resonant frequency with known capacitance (a) Circuit diagram (b) Result: Impedance versus frequency plot

From this result, new value of capacitors needed to tune the coil to desired frequency was calculated as shown below.

Let,

C_{1t} = initial total capacitance of the circuit;

C_{2t} = desired total capacitance of the circuit;

f_{1t} = initial frequency of resonance;

f_{2t} = desired frequency of resonance;

n = number of capacitors

$$C_{1t}f_1^2 = C_{2t}f_2^2$$

$$C_{1t} = \frac{C_1}{n_1} = \frac{32.2}{4} = 8.05 \text{ pF} ; f_1 = 138.656 \text{ MHz} ; f_2 = 128 \text{ MHz}$$

$$\therefore C_{2t} = \frac{C_{1t}f_1^2}{f_2^2} = 9.446 \text{ pF}$$

$$C_2 = C_{2t} \times n_2 = 9.446 \times 3 = 28.34 \text{ pF}$$

Coil 1 was now excited as shown in Figure 9(a) using a series resonating circuit by a broadband excitation. The results shown in Figure 9(b) showed that the resonant frequency was at 128.1MHz and effective series resistance of the coil (R_s) at this frequency with the tissue block at 8mm was 6.6 Ω .

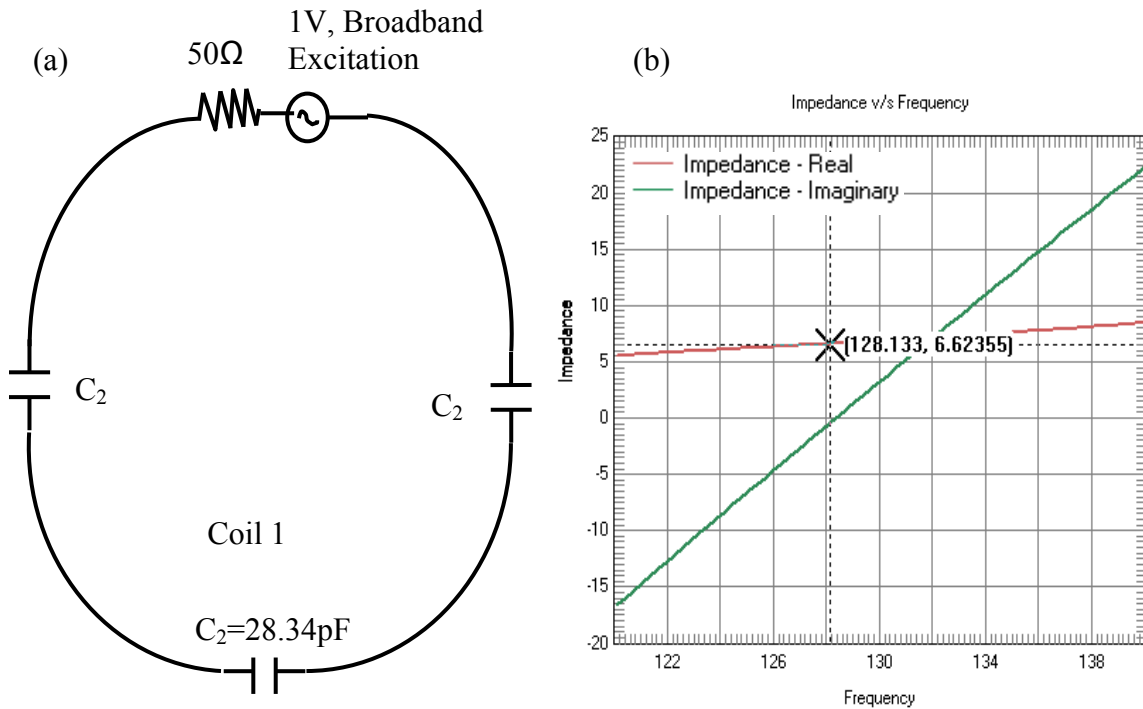


Figure 9 Preliminary simulation to find series resistance of the coil (a) Circuit diagram (b) Result: Impedance versus frequency plot – Series resistance (R_s) = 6.6Ω

Once the series resistance was known, the value of matching (C_m) and tuning capacitors (C') and inductor (L) that forms the part of preamplifier decoupling network was calculated as follows:

$$C_m = \frac{1}{\omega \sqrt{50 R_s}} = \frac{1}{2 \pi (128 \text{ MHz}) \sqrt{50 (6.6)}} = 68.45 \text{ pF}$$

$$L = \frac{1}{\omega^2 C_m} = 22.56 \text{ nH}$$

$$\frac{1}{C_{total}} = \frac{1}{C_m} + \frac{n-1}{C'}$$

where $C_{total} = C_{2t}$ is the net capacitance needed in the loop to tune the coil to desired frequency. The value of C_{total} was 9.446pF for all simulations at 3T and 40.418pF at 1.5T.

$$C' = \frac{n-1}{(C_{total}^{-1} - C_m^{-1})} = \frac{4-1}{(9.446 \text{ pF}^{-1} - 68.45 \text{ pF}^{-1})} = 32.87 \text{ pF}$$

Using these circuit parameters, coil 1 was excited with sinusoidal input at frequency f as shown in Figure 10(a) to verify tuning and matching of the coil. The result shown in Figure 10(b) shows that coil one was fairly matched and tuned.

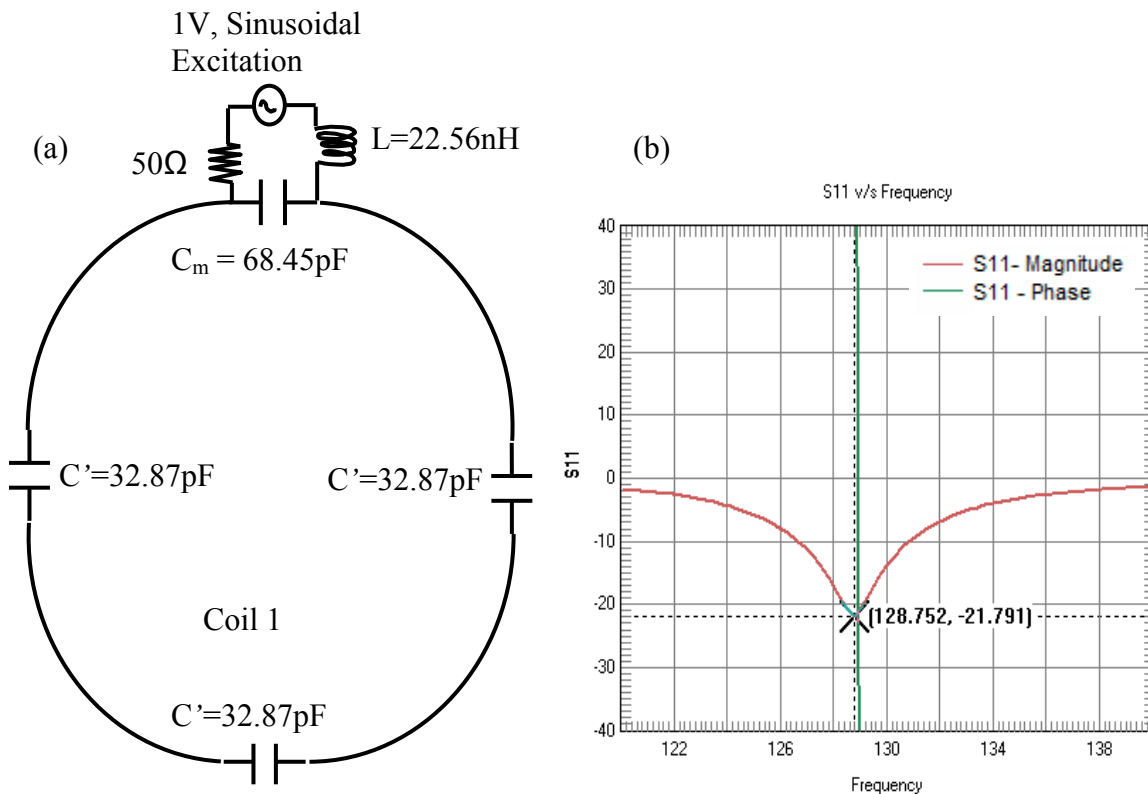


Figure 10 Simulation to verify matching and tuning of the coil (a) Circuit diagram (b) Result: S_{11} versus frequency plot

2. Simulations for SNR Modeling

As shown in Figure 11, coil 1 was matched to 50Ω and excited by a sinusoidal RF source with the frequency f ; coil 2 was terminated with same matching inductor and a resistor R to simulate the preamplifier input impedance, thus applying the well known preamplifier decoupling technique introduced by Roemer.

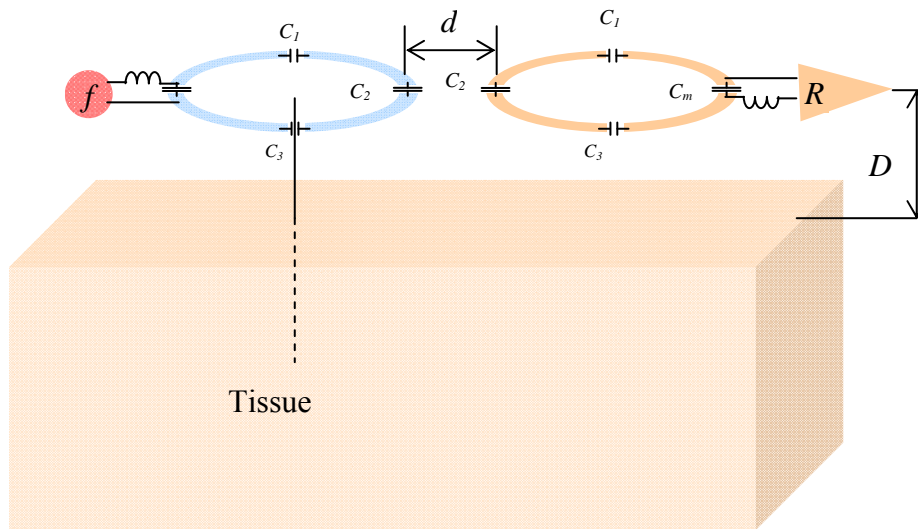


Figure 11 Graphical model consisting of two coils loaded with tissue block. Experimental variables are system frequency f , inter coil distance d , coil to phantom distance D and preamplifier input impedance R

Coil to tissue distance D and coil to coil distance d were varied to study the effect of different loading conditions and coil separation on SNR with different preamplifier resistances. Additionally, d was also set to infinity by removing coil 2 to obtain an SNR reference for comparison, referred to as “Baseline SNR”. Different values of f , R , d and D , which were used in this study, are shown in Table 1.

Table 1 Experimental parameters for FDTD simulations and their values

Experimental Parameters	Values
Frequency f (MHz)	64, 128
Preamplifier input impedance R (Ω)	3, 9
Inter coil distance d (mm)	-20 to +30 step 5, infinity
Load distance D (mm)	8, 16, 24

Circuit diagram for simulations done at 3T and 1.5T is shown in Figure 12 and Figure 13 respectively. Component values are given in Table 2 and Table 3 respectively. In 1.5T version, there are 2 capacitors per loop, but in 3T version, there are 4 capacitors per loop to keep the junction capacitance above 30pF.

Here, 3Ω resistor represents coil integrated preamplifier while 9Ω resistor represents preamplifier placed at the end of coaxial cable. Comparison of SNR studies between these two cases would show the effects on SNR due to preamplifier placement.

Table 2 Component values for FDTD modeling at 3T

	Coil to Phantom Distance		
	8mm	16mm	24mm
C_m	68.45pF	87.46pF	111.91pF
L	22.56nH	17.47nH	13.65nH
C'	32.87pF	31.76pF	30.95pF

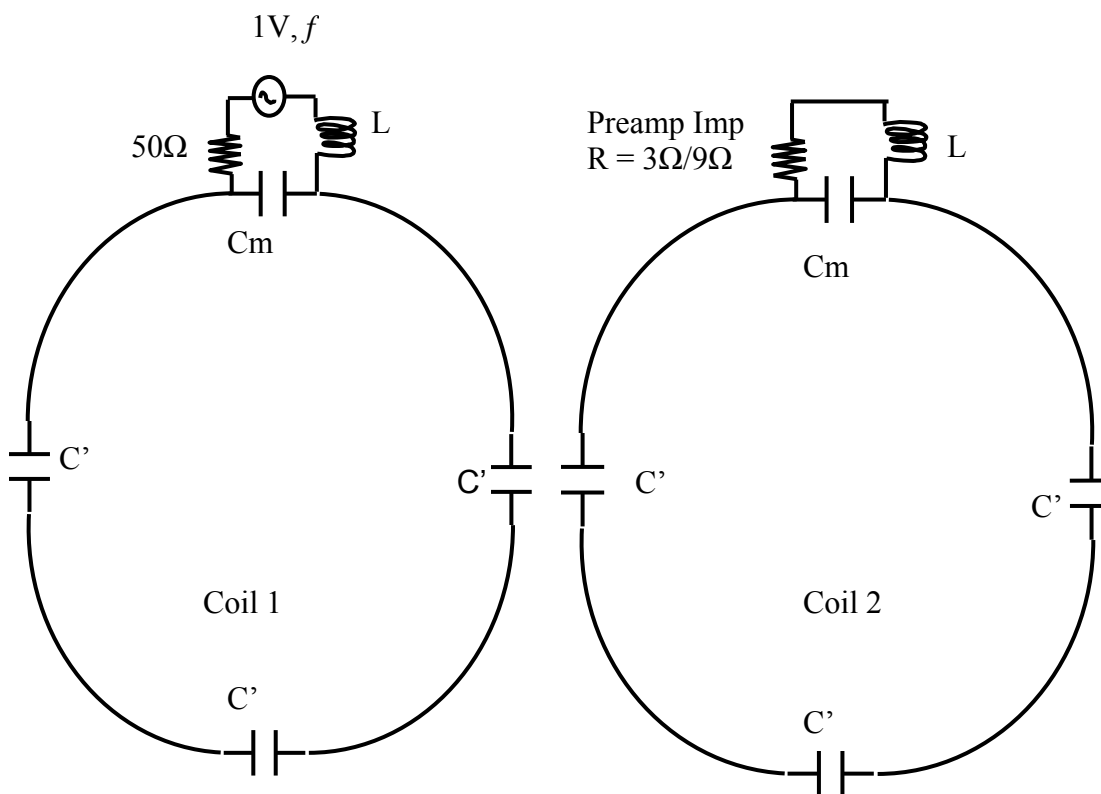
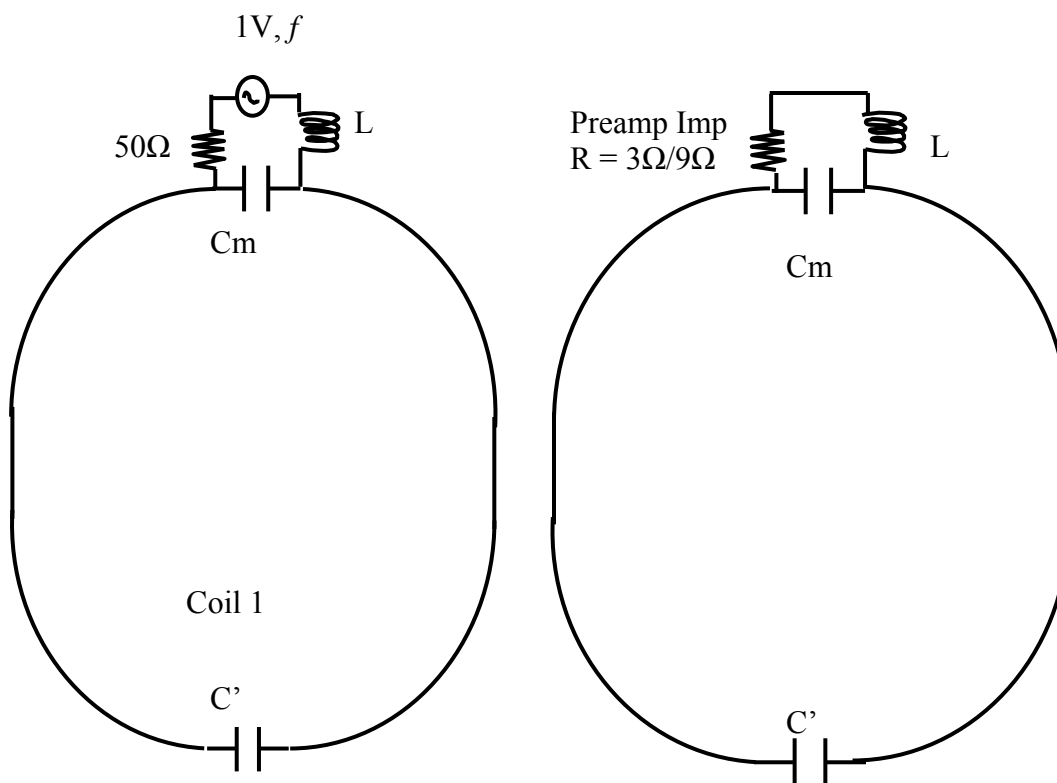
Figure 12 Circuit diagram for FDTD simulations at 3T ($f = 128.752\text{MHz}$)

Table 3 Component values for FDTD modeling at 1.5T

	Coil to Phantom Distance		
	8mm	16mm	24mm
C_m	306.01pF	390.68pF	487.25pF
L	21.18nH	16.59nH	13.3nH
C'	46.57pF	45.08pF	44.07pF

Figure 13 Circuit diagram for FDTD simulations at 1.5T ($f = 63.8\text{MHz}$)

3. SNR Estimation

Signal to Noise Ratio (SNR) was estimated in FDTD by employing the Principle of Reciprocity which was first introduced by Hoult^{35,46} as a strategy assessing nuclear magnetic resonance (NMR) signal strength. In NMR context, the Reciprocity theorem in simple terms states that if a direct current were applied to a receiving coil and the B_1 field created by it at the NMR sample were measured, the signal S induced in the coil by the precessing nuclear magnetic moment would be proportional to the strength of this hypothetical field.

Signal to Noise Ratio can be given by:

$$SNR = \frac{Signal}{Noise} = \frac{-\frac{d}{dt} \int \frac{\vec{B}_1}{I} \cdot \vec{M} dV}{\sqrt{4kTR\Delta f}}$$

where $\frac{\vec{B}_1}{I}$ is the magnetic field produced at volume element dV by a surface coil carrying unit current, \vec{M} is magnetization per unit volume assumed to be in direction perpendicular to main magnetic field \vec{B}_0 , k is Boltzmann constant, T is absolute temperature in Kelvin and R is resistance.

The integral in the above equation can be assumed to be over a small volume, where B_1 is assumed to be constant. \vec{M} is constant at a given field strength and other factors k , T , Δf are constant Thus, SNR can be written as:

$$SNR \propto \frac{B_1/I}{\sqrt{R}} = \frac{B_1}{\sqrt{P_{dis}}} \quad \text{where } P_{dis} \text{ is dissipated power.}$$

For all the simulations for SNR modeling, snapshot of B_1 field was obtained in a plane perpendicular to the plane of coil and passing through the axis as shown in Figure

14. Remcom Inc. uses open file format for output data, so the results were requested using Matlab script. Therefore, the B1 field data for each simulation were also stored in data files with *.bfd* extension while the dissipated power values were stored in data files with *.pdis* and *.ssout* extension. The dissipated power values in *.pdis* files were different from the one stored in *.ssout* file for most of the simulations.

However, upon discussions with Remcom, it was clarified that the values displayed by the software were the correct values. Therefore, for all SNR calculations, the dissipated power values stored in *.ssout* files were taken into consideration.

Remcom provided the scripts that would also calculate rotating components (B_1^+ and B_1^-) of the B1 field using *.bfd* files. The B_1^+ and B_1^- field data were stored in data files with extension *.rot.bfd*. Snapshots of these fields were also obtained.

Matlab scripts given in Appendix A were written to read these data files and obtain various plots.

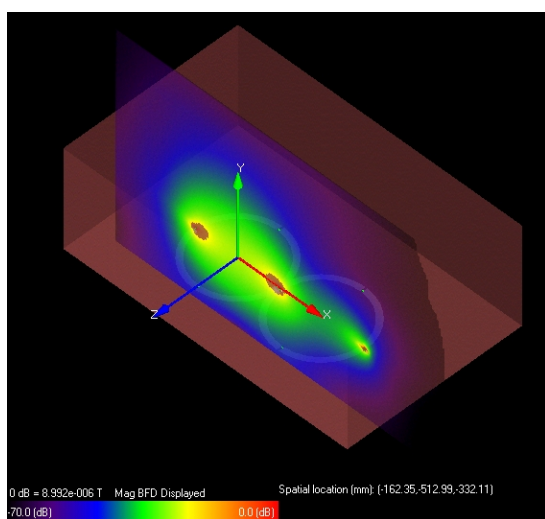


Figure 14 Typical FDTD result: Snapshot of B_1 field magnitude in plane perpendicular to plane of coil

B. Bench Measurements at 3T and 1.5T

1. Experimental Setup

Bench Measurement was done using the setup shown in Figure 15. Both coils were constructed and loaded by a phantom of 15 X 15 X 38cm. The phantom contained 3.368g/L $\text{NiCl}_2 \cdot 6\text{H}_2\text{O}$ and 2.4g/L NaCl, consistent with the loading of the tissue block used in the FDTD simulation.

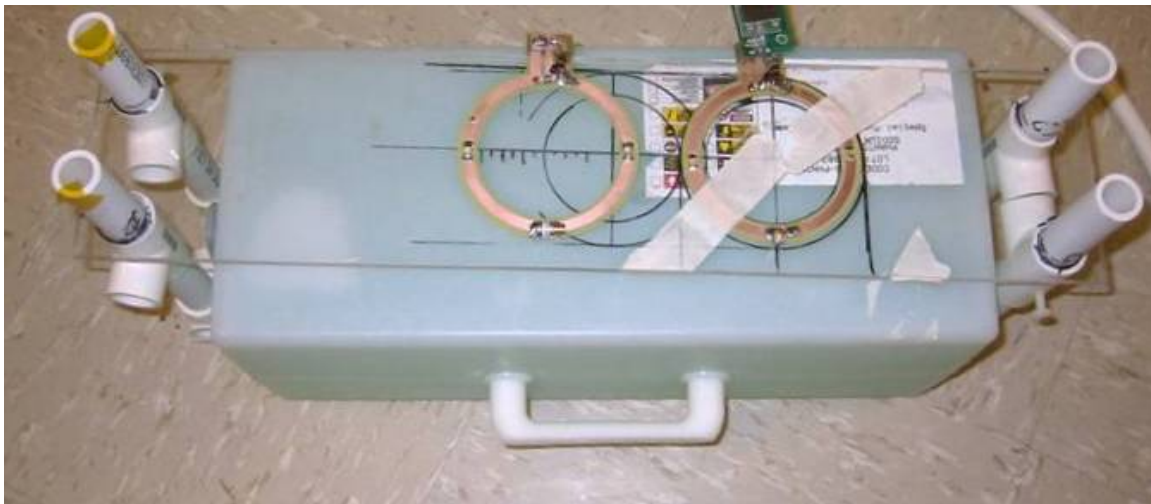


Figure 15 Bench experiment: Actual setup

To ensure that the coils in the bench experiment have similar loading condition as in FDTD, the coil to phantom distance D was adjusted such that the Q of the coil for the bench measurement, measured by using two flux probes, matched the Q of the coil calculated from FDTD simulation. The coil to phantom distance in the bench measurement adjusted by this method matched the FDTD value.

Calculation of Q value for a typical case 3T 8mm is shown here.

As shown in Figure 16, channel 1 of the network analyzer was connected to coil 1, matched to 50Ω and tuned to desired frequency f in absence of coil 2, at a constant power level of 0dBm and channel 2 was connected to a small flux probe placed at a distance of 25mm from the coil 1 along its axis on the opposite side of the phantom.

2. SNR Estimation

SNR was estimated by measuring S_{21} between coil 1 and the flux probe while varying f , d , D and R . Reflections at port 1 were taken into account so that the perceived drop in S_{21} was all due to coupling and not due to reflection. Therefore, corrections were made for reflected power by measuring the forward reflection co-efficient - S_{11} . In FDTD reflections at port 1 were accounted for, since it calculated dissipated power independent of match. Calculation of SNR from S_{11} and S_{21} measurement is shown below:

Input power level $P = 0 \text{ dB}_m = 1\text{mW}$

Reflected power at port 1: $P \left(10^{\frac{S_{11}}{10}} \right)$

Net input power to coil 1 at port 1: $P_{in(net)} = P \left(1 - 10^{\frac{S_{11}}{10}} \right)$

Power received by flux probe at port 2: $P_{rec} = P \left(10^{\frac{S_{21}}{10}} \right)$

$S_{21(\text{corrected})}$ (correction for reflection at port 1): $10 \left[\text{Log}_{10} \left(\frac{P_{rec}}{P_{in(net)}} \right) \right]$

$S_{21(\text{corrected})}$ with coil 2 placed at infinity (coil 2 absent) = $S_{21(\text{corrected})}(\infty) = \text{Base SNR}$

SNR drop due to presence of coil 2 at distance d from coil 1 = $S_{21(\text{corrected})}(d) - \text{Base SNR}$

C. Bench Measurements at 4.7T

Two 76.2mm diameter loop coils with 5.08mm width were constructed from FR04 using C30 PC Board Prototyper (LPKF, Wilsonville OR) as shown in Figure 17. The coils were loaded with semi-cylindrical phantom of diameter 127mm and length 304.8mm filled with 3.368g/L $\text{NiCl}_2 \cdot 6\text{H}_2\text{O}$ and 2.4g/L NaCl solution at a distance of 8mm as shown in Figure 18.

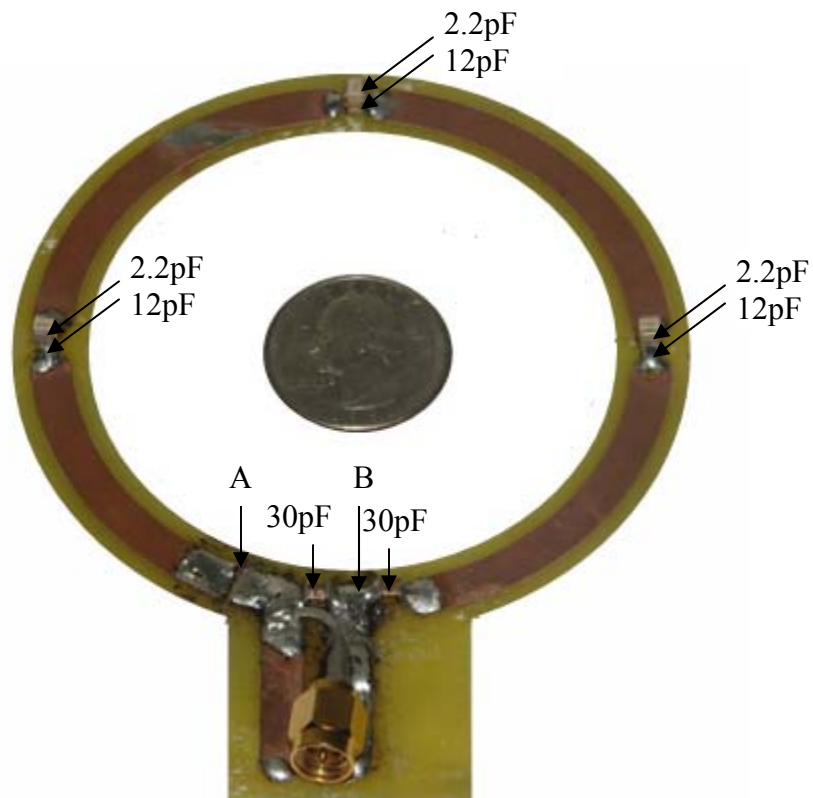


Figure 17 3" Loop coil for experiments at 4.7T

The setup described above was placed inside a 12 rung birdcage coil made of copper tape constructed at Magnetic Resonance Systems Lab (MRSL, College Station-TX) to closely simulate the NMR experiment. Specifications for the birdcage coil are given in the Table 5. Birdcage coil was properly detuned by applying a bias voltage to PIN diode circuit. The coils were then matched to 50Ω and tuned to 200.228MHz under this loading condition using capacitors shown in Figure 17.

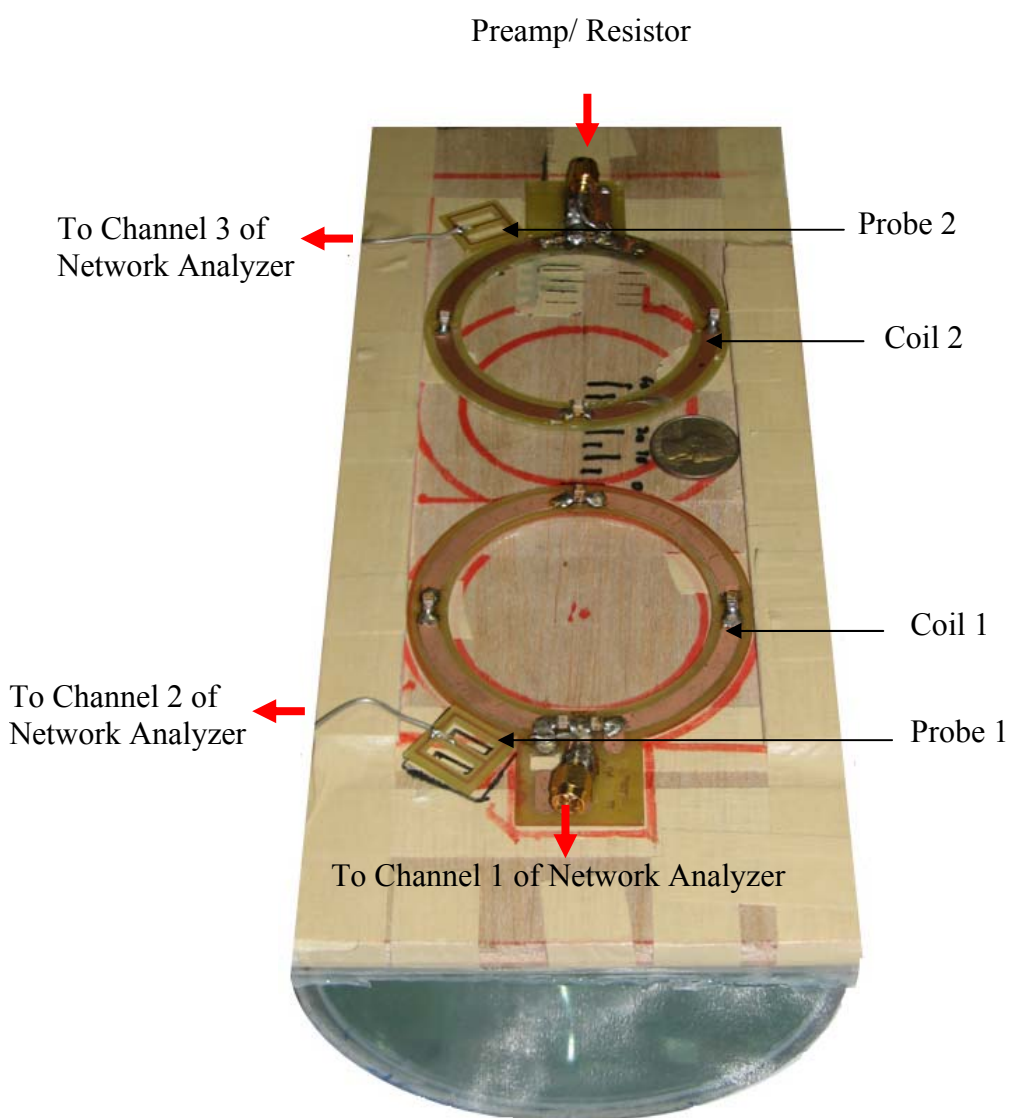


Figure 18 Experimental setup for bench measurements at 4.7T

Table 5 Birdcage coil specification

Parameter	Value
Birdcage Coil Diameter	152.4mm
Birdcage Coil Length	228.6mm
Birdcage Shield Diameter	177.8mm
Birdcage Shield Length	304.8mm
Birdcage Element Thickness	12.7mm
Capacitor Value	22pF

Coil 1 was excited by connecting it to channel 1 of Agilent E5071C ENA Series Network Analyzer (Agilent Technologies Inc, Santa Clara-CA). Coil 2 was terminated with different preamplifiers and resistors as shown in Figure 19. Figure 19 also shows the impedance measured at the coil terminals across AB (Figure 17) for each case. While measuring the impedance, the coil was disconnected at points A and B. The capacitor between AB was removed and the impedance was again measured.

Figure 20 shows low impedance and standard 50Ω preamplifier used for these experiments. Both the preamplifiers were tested for their input impedance and gain. Low impedance preamplifier ($\sim 3\Omega$) was procured from Microwave Technology Inc., (Fremont, CA) while standard preamplifier ($\sim 50\Omega$) was made in Magnetic Resonance Systems Lab using Gali 74+ IC obtained from Minicircuits (Brooklyn, NY).

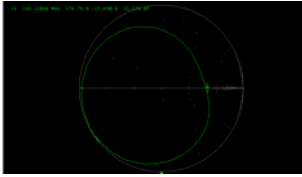
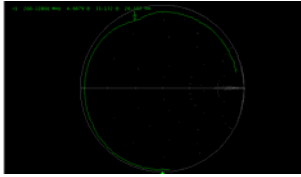
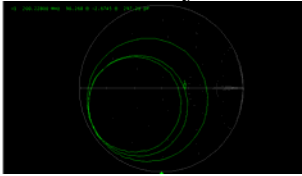
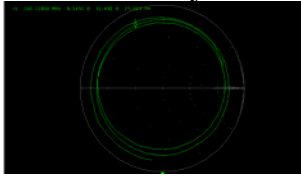
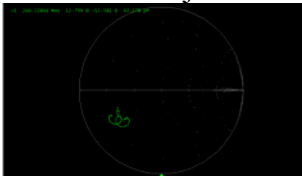

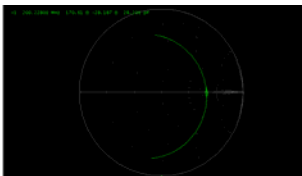
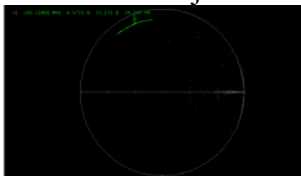
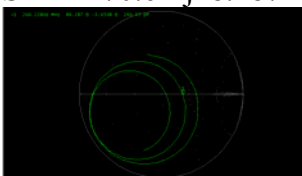
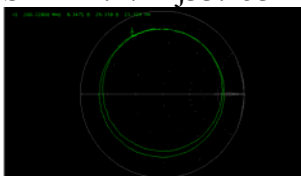
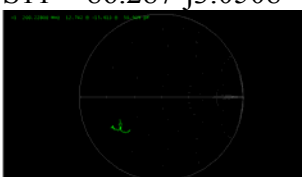

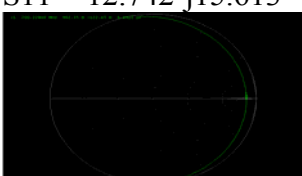

Coil 2 termination	Impedance at the coil terminal	Impedance at the coil terminal with capacitor removed
1) 3Ω preamplifier placed on the coil	 $S_{11} = 174.76 - j25.498$	 $S_{11} = 4.6679 + j33.152$
2) 3Ω preamplifier placed at the end of 2λ coaxial cable	 $S_{11} = 90.268 - j2.6745$	 $S_{11} = 8.1492 + j31.481$
3) 50Ω preamplifier placed at the end of 2λ coaxial cable	 $S_{11} = 12.799 - j12.581$	 $S_{11} = 38.666 + j5.7016$
4) 3Ω resistor placed on the coil	 $S_{11} = 170.61 - j28.187$	 $S_{11} = 4.172 + j33.153$
5) 3Ω resistor placed at the end of 2λ coaxial cable	 $S_{11} = 86.287 - j3.0508$	 $S_{11} = 8.3471 + j29.358$
6) 50Ω resistor placed at the end of 2λ coaxial cable	 $S_{11} = 12.742 - j15.613$	 $S_{11} = 45.122 + j10.189$
7) 0Ω resistor placed on the coil	 $S_{11} = 962.35 - j122.45$	 $S_{11} = 0.744 + j25.657$

Figure 19 Experimental cases for coil 2 termination

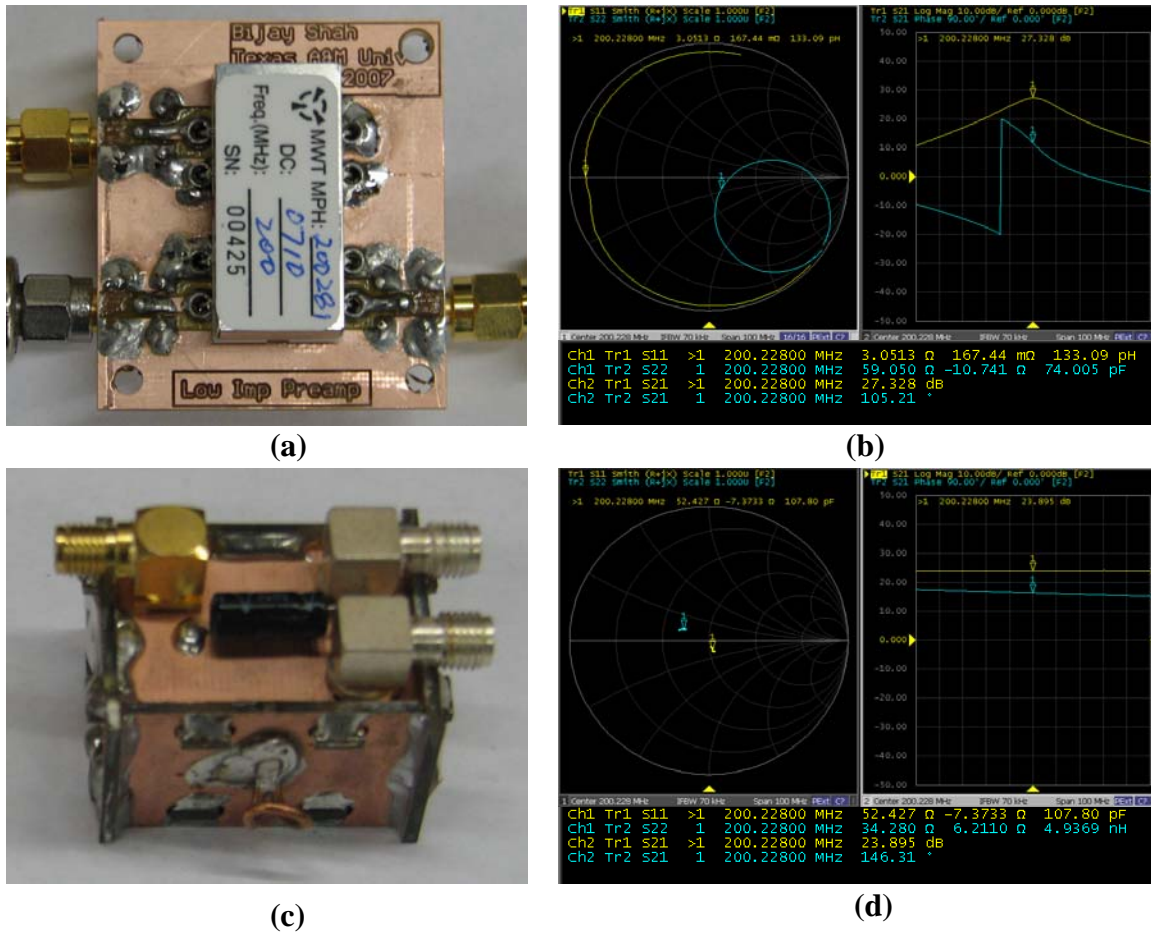


Figure 20 (a) Low input impedance preamplifier (b) Test results: Input impedance = $(3.05 - j0.1)\Omega$; Gain 27.32dB (c) Standard 50Ω preamplifier (d) Test results: Input impedance = $(52.42 - j7.3)\Omega$; Gain = 23.89dB

Figure 21 shows two different configurations for preamplifier placement. Baluns were used when preamplifiers were placed at the end of coaxial cable to prevent the shield currents.

Initial set of experiment, experiment A, was done for case 1 through 6 to compare the results obtained using preamplifier and using resistor equivalent to input impedance of preamplifier. A second set of experiment, experiment B, was done for case 7 to get an idea of the best case of preamplifier decoupling. However, experiments for case 4 through 6 were repeated so that they can be compared with case 7.

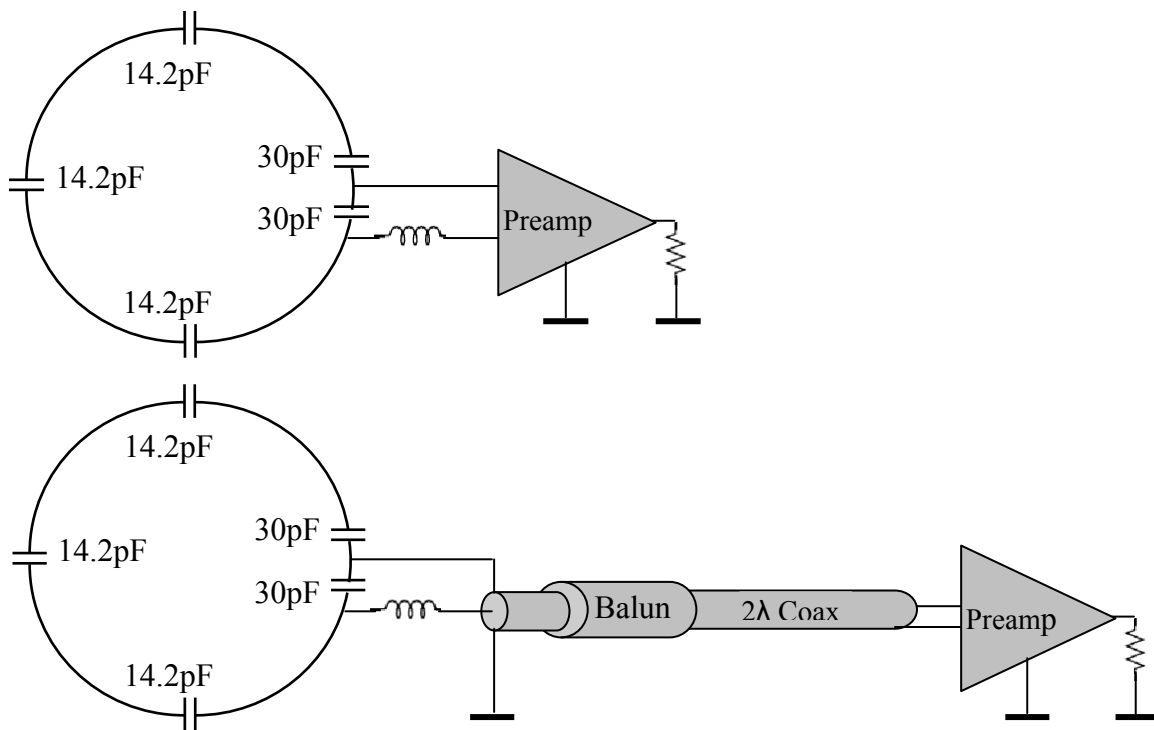


Figure 21 Schematic diagrams: Preamplifier placement a) Preamplifier placed on the coil
b) Preamplifier placed at the end of 2λ coaxial cable

Current in coil 1 was measured using a planar pair flux probe placed near to coil 1 and connected to channel 2 of the network analyzer. Similarly current in coil 2 was measured using a similar planar pair probe placed near coil 2 and connected to channel 3 of the network analyzer. To amplify low signals picked up by these probes, a dual channel 20dB amplifier (8847A OPT 001 Dual Amplifier 0.1-400MHz HP Gain 20dB 2 Channel) was used to connect both the probes to the network analyzer. S_{11} , S_{21} and S_{31} parameters were measured for different inter-coil distances. The difference ($S_{31} - S_{21}$) would give an estimation of ratio of currents in coil 2 and coil 1 as follows:

$$\frac{I_2}{I_1} = 10^{\left[\frac{S_{31} - S_{21}}{20} \right]}$$

CHAPTER IV

RESULTS AND DISCUSSIONS

A. Finite Difference Time Domain Modeling

Figure 22 shows the SNR with increasing distance along the axis of coil 1 obtained from 12 different FDTD simulations for each inter-coil distance d for a typical case – $B_0 = 3\text{T}$, $D=24\text{mm}$, $R=9\Omega$. It can be seen that SNR decreases along the axis of coil 1.

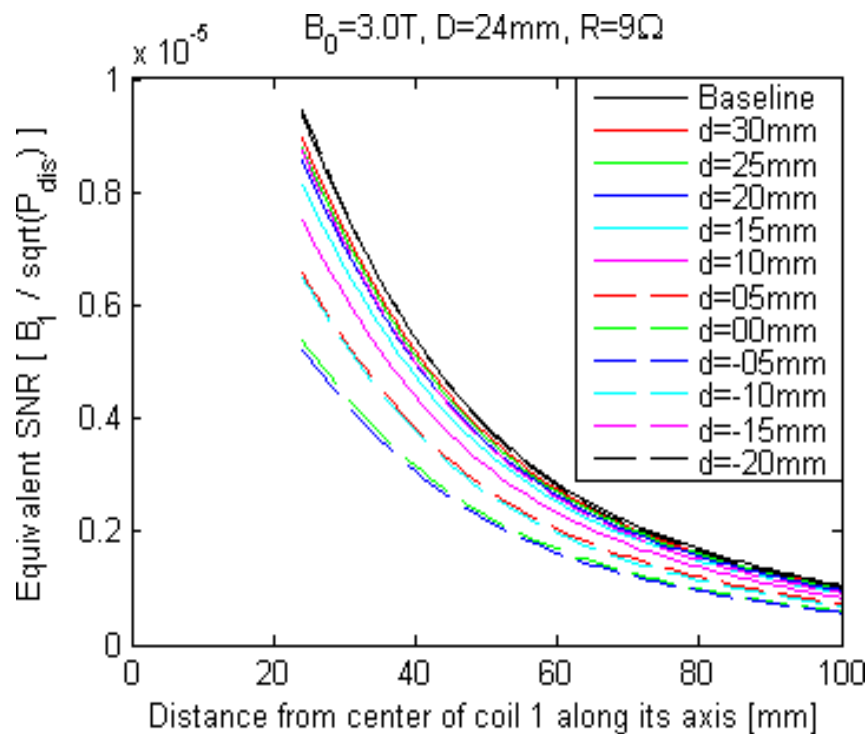


Figure 22 FDTD simulation results: SNR vs. distance from center of coil 1 along its axis [mm]

SNR drop in dB for the above case is shown in Figure 23. Black curve represents the case when coil 2 is absent (Coil 2 at infinity) and is considered as baseline for reference. As inter-coil distance is decreased from 30mm to -5mm, SNR decreased from 0dB to -5dB. It increased thereafter as the coils were brought closer to “magic overlap”.

The results show that SNR degradation is almost constant at any point along the axis of coil 1.

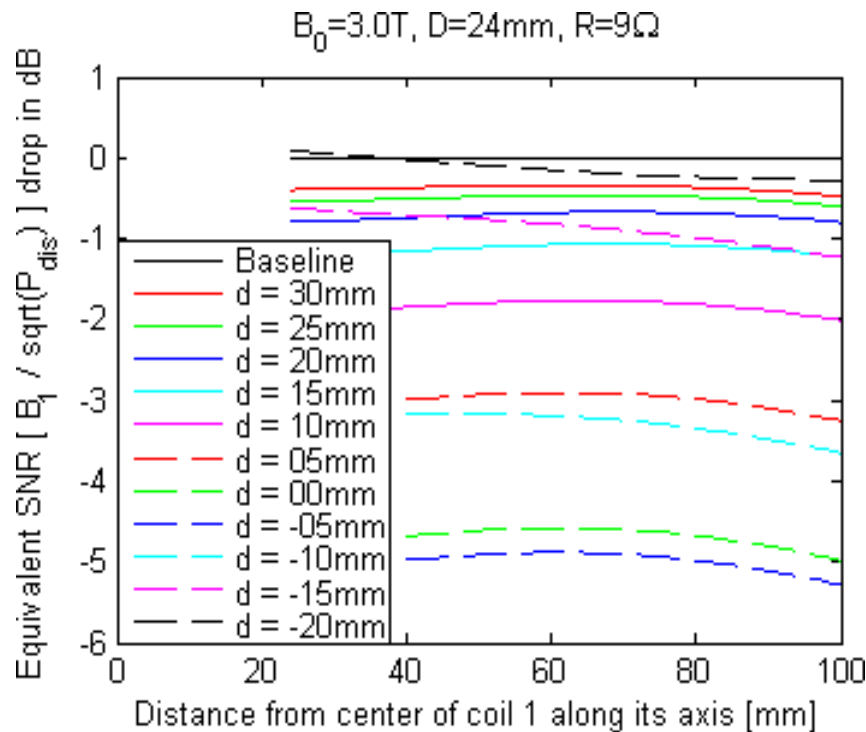


Figure 23 FDTD simulation results: SNR drop in dB vs. distance from center of coil 1 along its axis [mm]

Therefore, each line was represented by a single value, and all FDTD simulation results were plotted together as shown in Figure 24. Results shown in Figure 22 and Figure 23 and are now represented by the black dashed line in Figure 24. Figure 25 demonstrates SNR drop in dB along any point on axis of coil 1 as a function of inter-coil distance d for 12 different combination of field strength B_0 , preamplifier input impedance R and coil to phantom distance D .

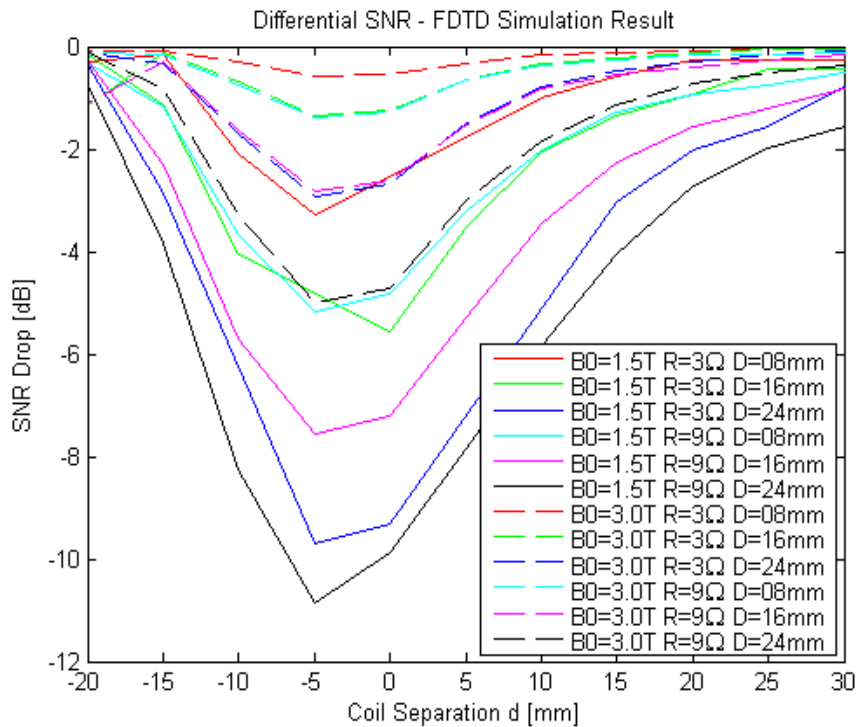


Figure 24 FDTD results: SNR drop in dB vs. coil separation for different combinations of B_0 , R and D

In addition to the above plots, profile of B_1 , B_1^+ and B_1^- field were also obtained for each simulation. Figure 25 shows the normalized B field profile obtained as a result of simulations at 3T as a function of preamplifier impedance (R) and array to phantom distance (D) for the inter-coil distance $d = 15$ mm. It is evident that, 3Ω cases show less coupling as compared to 9Ω cases. We, also see increased coupling between coils as the phantom is moved away from the coil. Figure 26 shows similar B field profile at 1.5T. A comparison of Figure 25 and Figure 26 indicates that coupling is severe at 1.5T. Figure 27 shows a comparison of B_1 , B_1^+ and B_1^- field at a typical case.

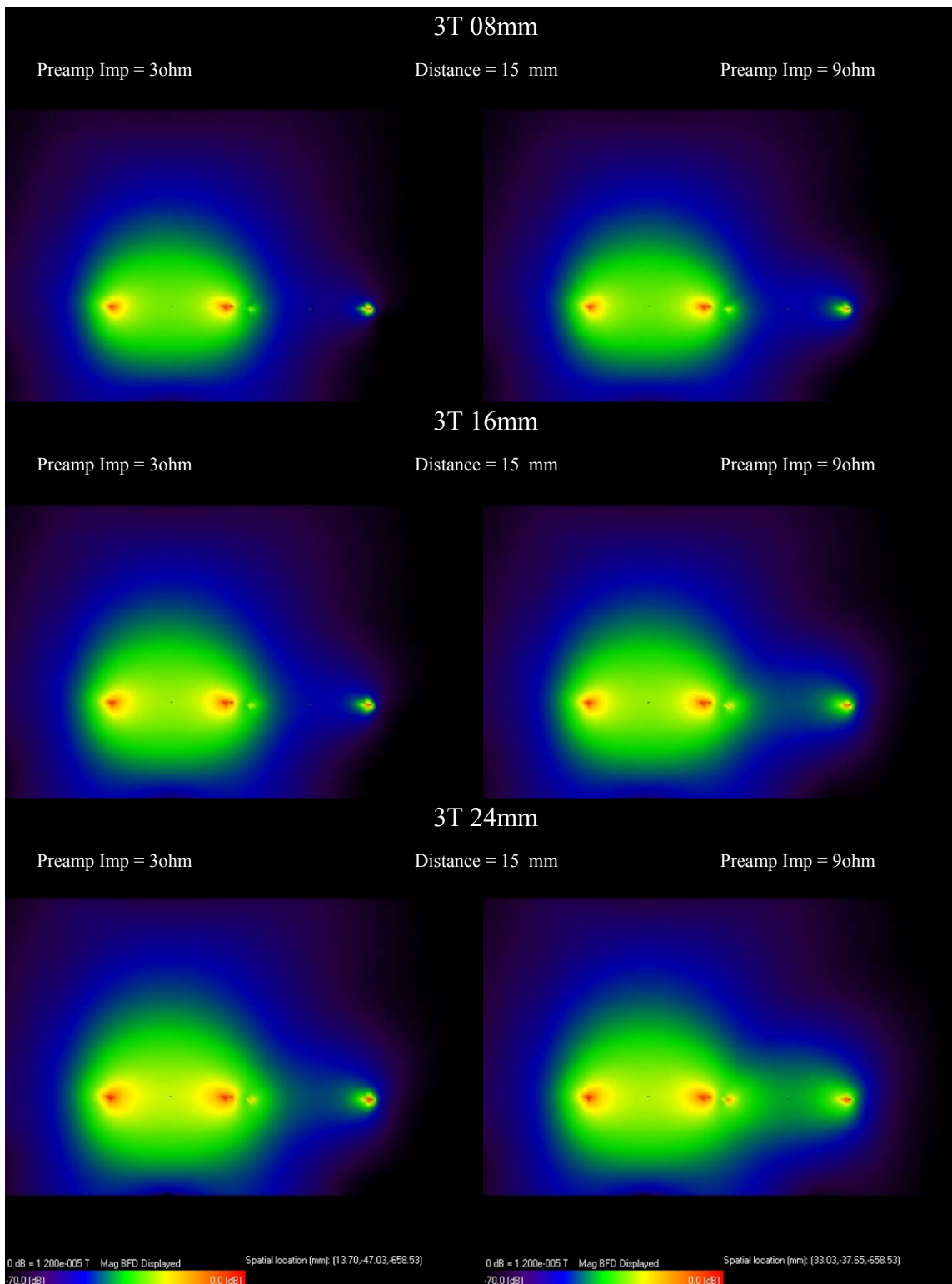


Figure 25 B_1 field profile as a function of preamplifier input impedance R and phantom distance D at 3T for inter-coil distance $d=15$ mm

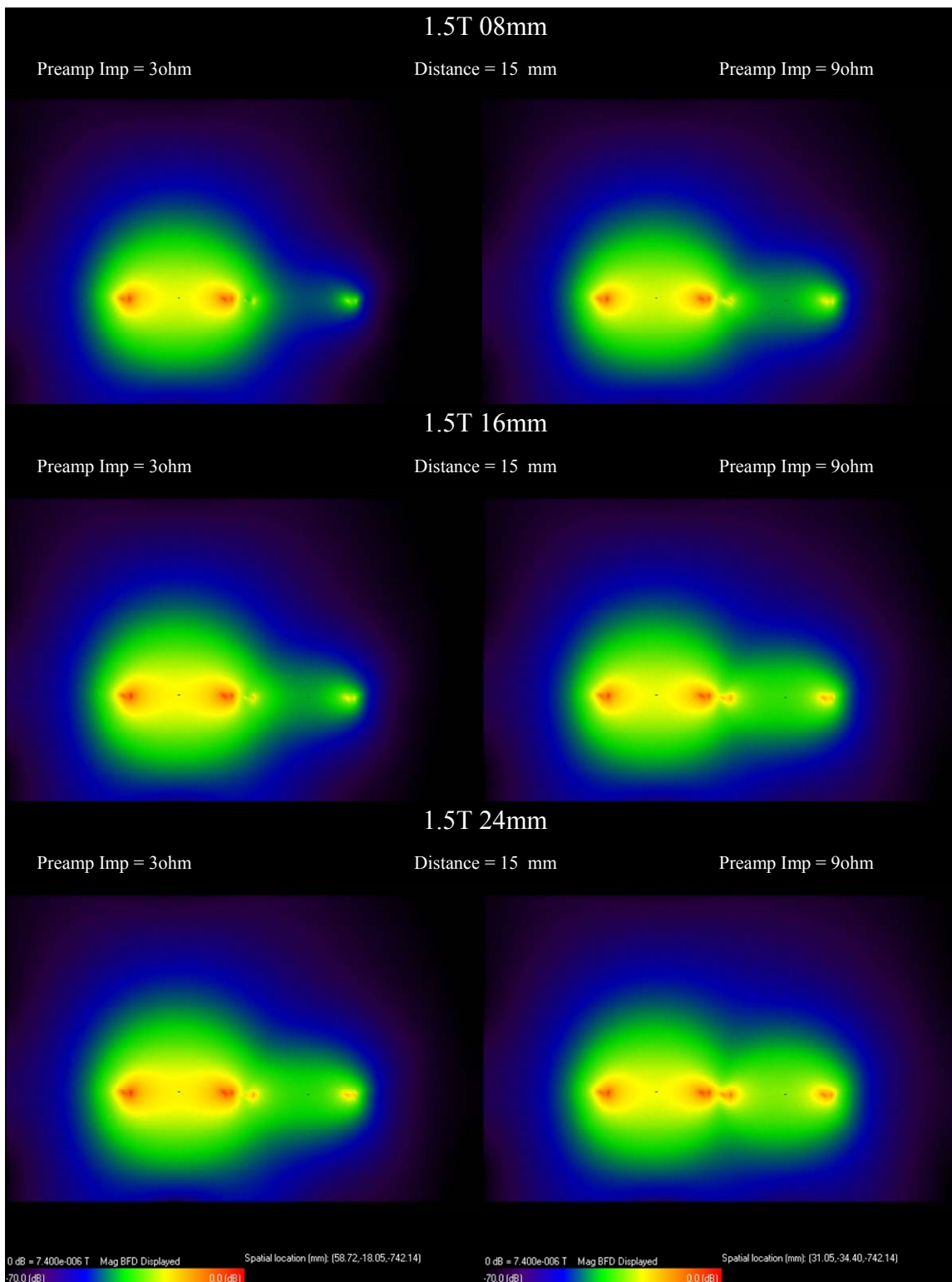


Figure 26 B_1 field profile as a function of preamplifier input impedance R and phantom distance D at 1.5T for inter-coil distance $d=15\text{mm}$

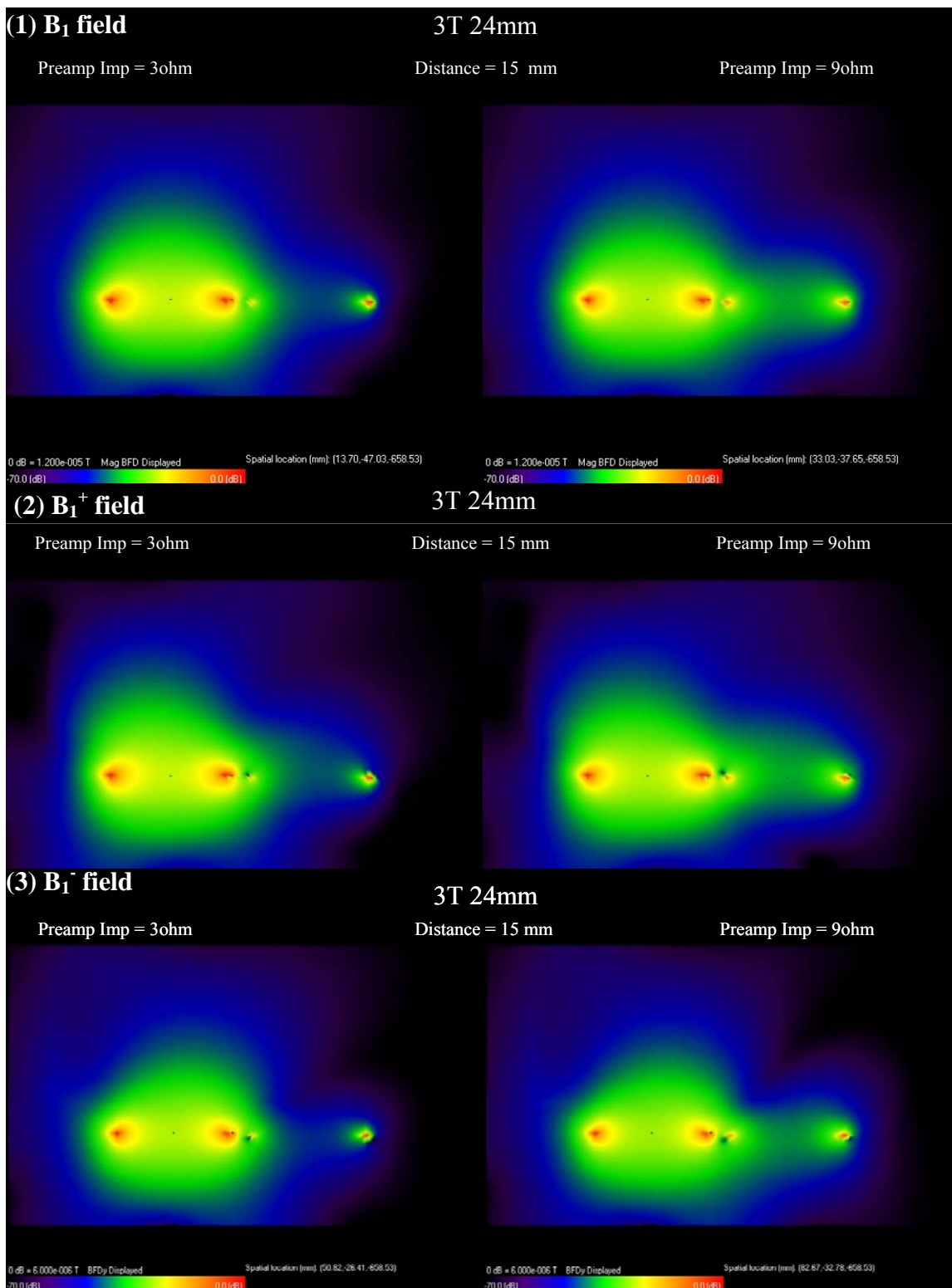


Figure 27 Comparison of B , B_1^+ and B_1^- field profile for the case $B_0 = 3\text{T}$, $D = 24\text{mm}$, $d = 15\text{mm}$

B. Bench Measurement

Figure 28 shows S_{11} plot obtained from Bench measurement experiment. It can be seen that deterioration (increase) in S_{11} is less at higher field strength, lower preamplifier input impedance and at lower coil to phantom distance.

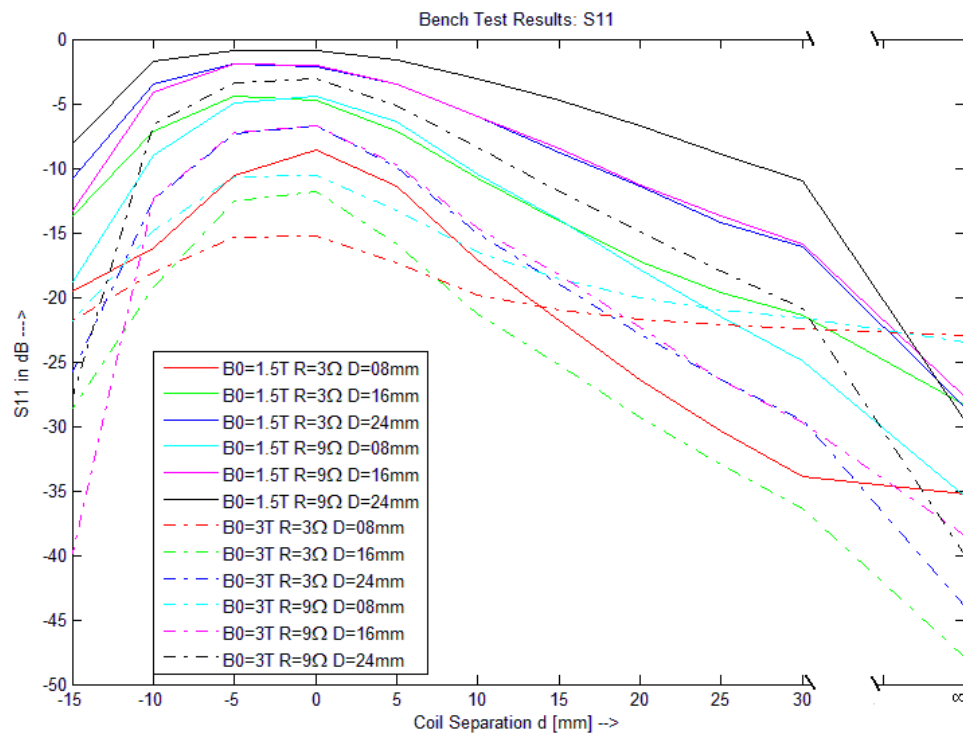


Figure 28 Bench measurement results: S_{11} in dB vs. coil separation for different combinations of B_0 , R and D

Figure 29 shows S_{21} plot in dB obtained from bench measurement. It is clear that drop in S_{21} is less at higher field strength, lower preamplifier input impedance and at a lower coil to phantom distance.

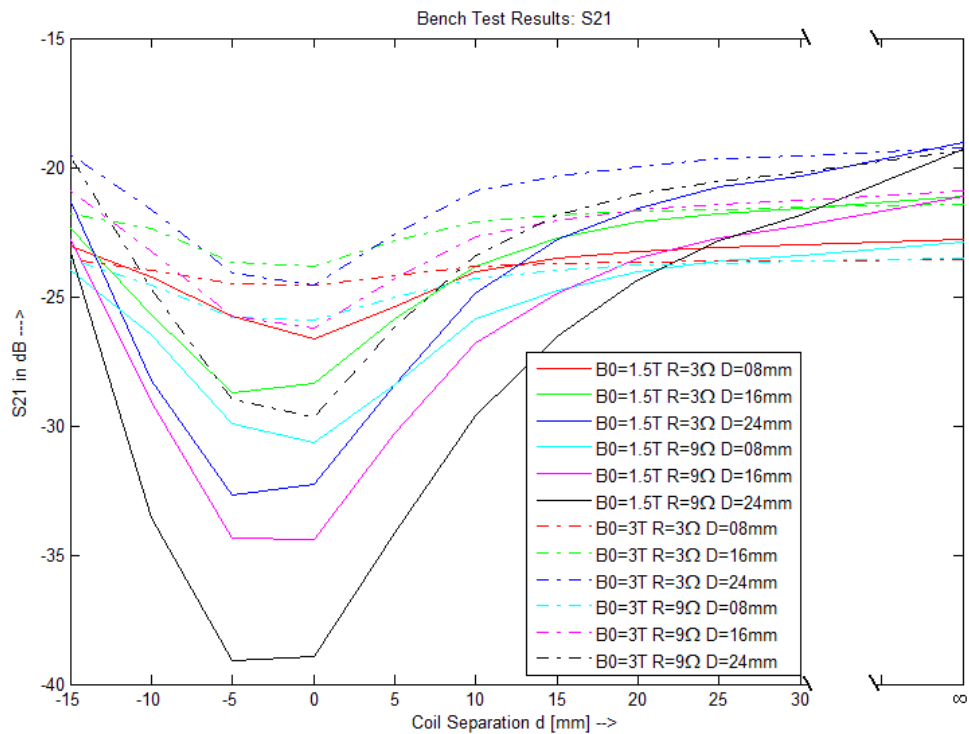


Figure 29 Bench measurement results: S_{21} in dB vs. coil separation for different combinations of B_0 , R and D

Figure 30 shows the SNR drop in dB obtained from bench measurement. Bench measurement results highly matched the results obtained from FDTD simulation.

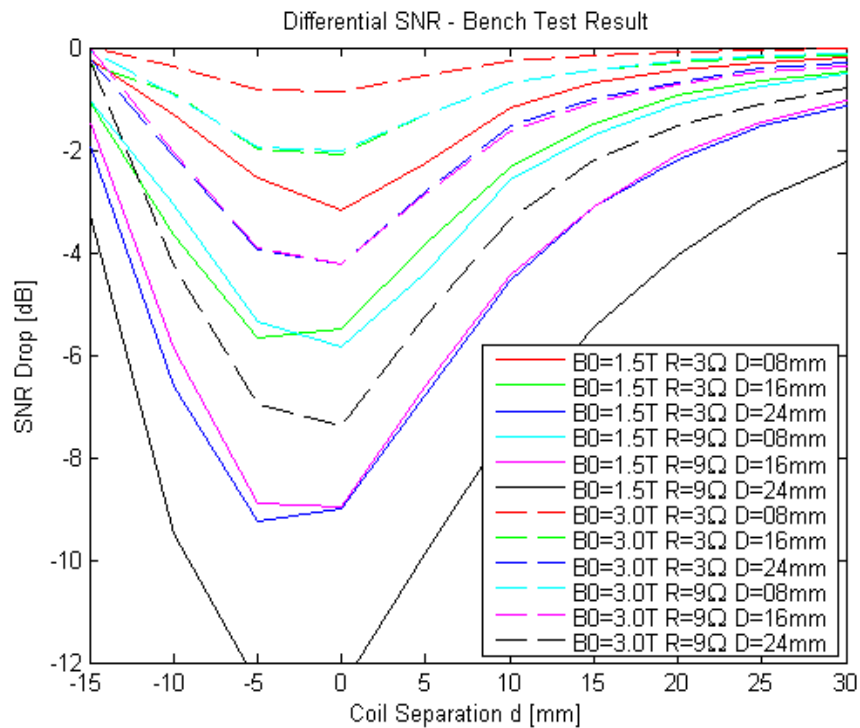


Figure 30 Bench measurement results: SNR drop in dB vs. coil separation for different combinations of B_0 , R and D

C. Other Results

SNR studies similar to FDTD and Bench experiments were also done using two other methods – Imaging experiment and ADS (Advanced Design System) Modeling⁴⁷.

Figure 31 shows the results obtained from ADS modeling.

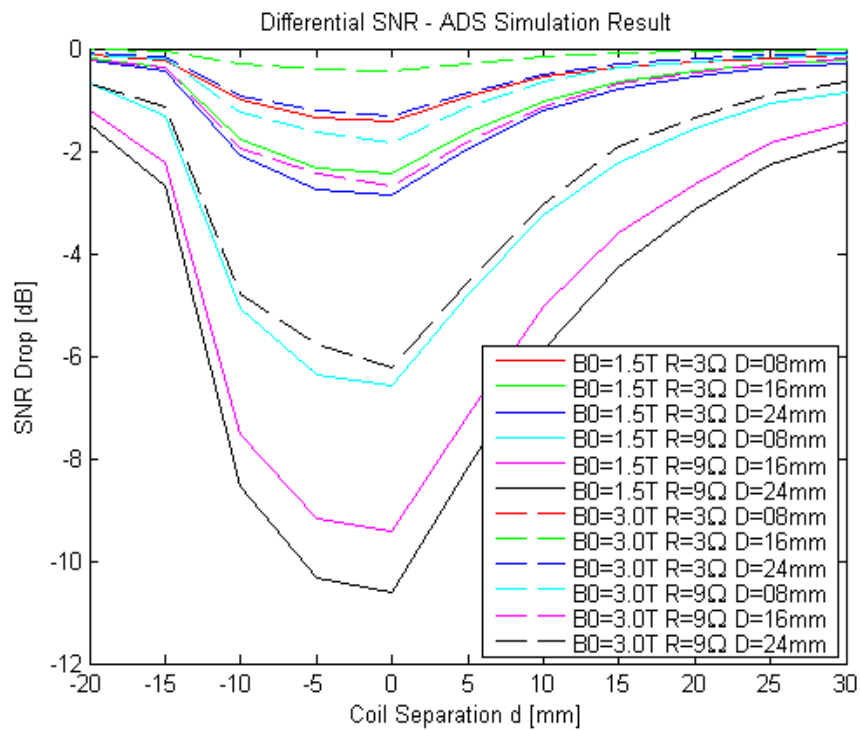


Figure 31 ADS modeling results: SNR drop in dB vs. coil separation for different combinations of B_0 , R and D

Figure 32 shows results for SNR studies obtained from imaging experiment.

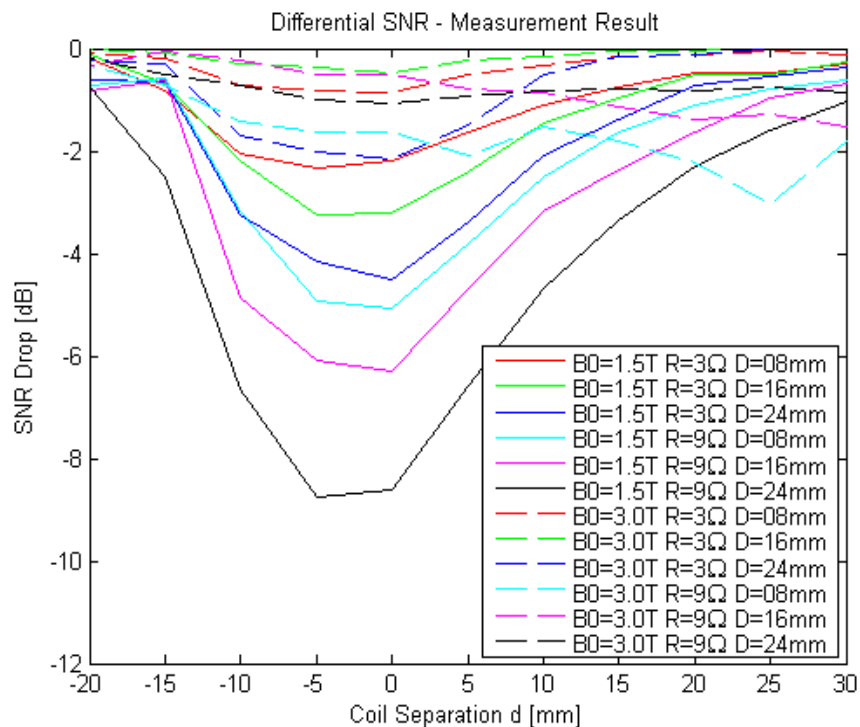


Figure 32 Imaging experiment result: SNR drop in dB vs. coil separation for different combinations of B0, R and D

All the methods for SNR studies at 3T and 1.5T gave similar results:

- Higher SNR drop for $R=9\Omega$ as compared to $R=3\Omega$
- Higher SNR drop at lower field strength (1.5T)
- Lower SNR drop for heavily loaded coils ($D=8\text{mm}$)
- Increase in SNR drop as coils are brought closer. Improvement in SNR when coils are closer to “magic overlap” where mutual inductance between two coils becomes zero.

D. Bench Measurement at 4.7T

Plots of S_{11} , S_{21} and S_{31} measurement for both experiment A and experiment B are given in Appendix B (figure B1-B6). Figure 33 shows plot of current ratio I_2/I_1 as a function of intercoil distance. Results obtained using preamplifiers are very similar to that obtained using resistor for most of the cases. Figure 34 shows current ratio plot for experiment B.

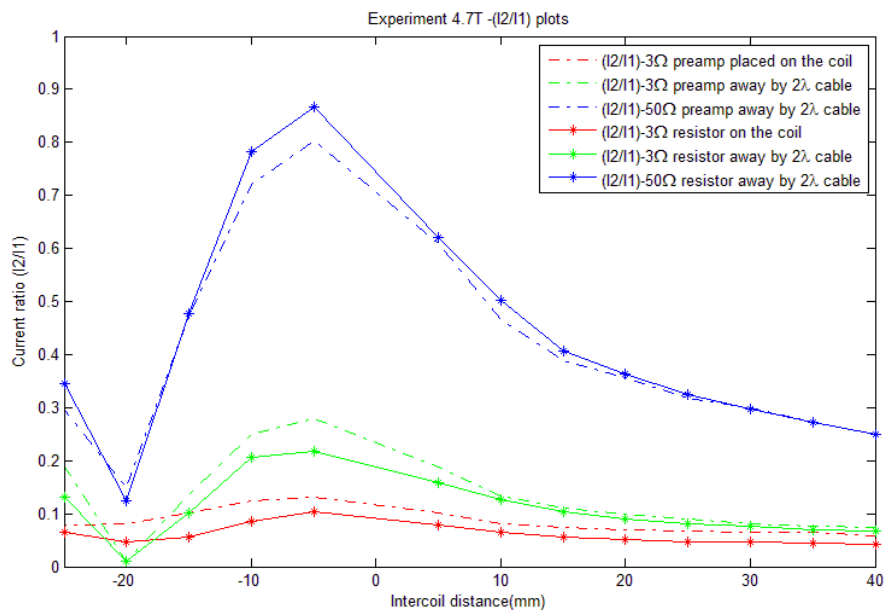


Figure 33 Experiment A results: Current ratio I_2/I_1 vs. intercoil distance

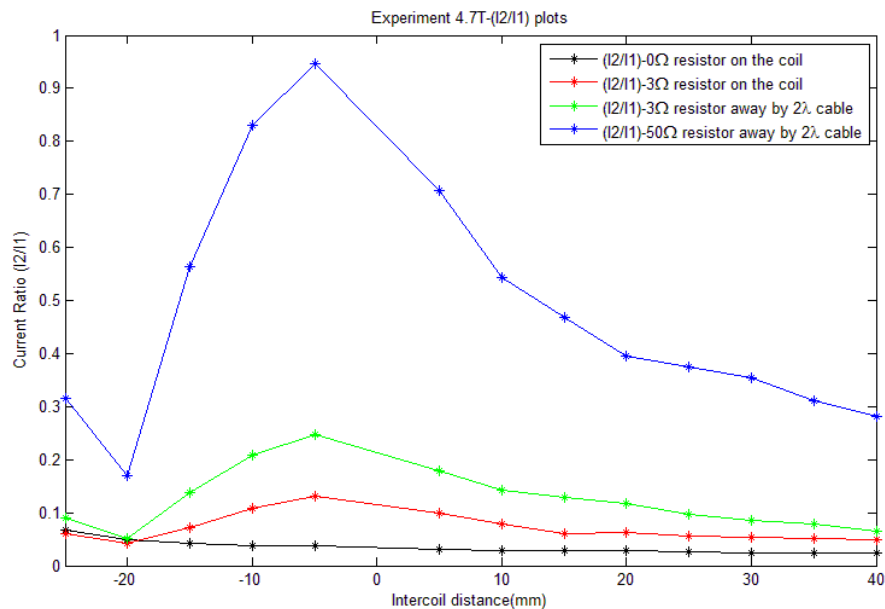


Figure 34 Experiment B results: Current ratio I_2/I_1 vs. inter coil distance

For all the cases, it can be seen the coupling between two coils increases as they are brought closer to one another. Coupling is maximum for $d = -5\text{mm}$. Coupling reduces dramatically for $d = -20\text{mm}$ because of cancellation of mutual inductance between two coils at the “magic overlap”.

It is evident that there exists strong coupling between two coils when 50Ω preamplifier is used at the end of 2λ coaxial cable. Low impedance preamplifier at the end of 2λ coaxial cable showed appreciable decoupling between two coils for $d > 20\text{mm}$ and for $d = -20\text{mm}$. As was expected, coils were better decoupled when low impedance preamplifiers were placed on the coil.

CHAPTER V

THESIS CONTRIBUTION

Considering that this thesis would be a good source of information for RF coil engineers, a summary of procedure to study coupling between two coils and metrics for making decision regarding the selection and placement of preamplifier is presented here. Methods presented here are based on bench measurements. However, modeling techniques based on similar methods can be used to predict the results before verifying it with bench measurements.

A. Procedure for Determining the Type and Placement of Preamplifier

- 1) Make two coils as per the specification given (Coil geometry).
- 2) Determine the coil to phantom distance (D) for which SNR for single coil is maximum. For this, follow the procedure described separately.
- 3) Match both the coils for this loading condition and tune it to desired frequency, independently.
- 4) Determine the inter-coil distance (d) which corresponds to distance between two next nearest coil elements in the array. For this, follow the procedure described separately.
- 5) Place two coils at an inter-coil distance d from each other and at a distance D from the phantom.
- 6) Use one of two methods to determine current ratio for all the following cases of preamplifier termination:
 - Case (A): 50Ω standard preamplifier at the end of coaxial cable
 - Case (B): Low impedance preamplifier at the end of coaxial cable
 - Case (C): Low impedance preamplifier on the coil

- 7) Use decision making procedure to determine the best configuration for preamplifier placement and type.

1. Finding Coil to Phantom Distance for Maximizing SNR

- 1) Load the coil with a phantom at an arbitrary distance from the coil as shown in Figure 35.
- 2) Match and tuned the coil for this condition.
- 3) Fix a pickup probe with the phantom as shown in figure.
- 4) Connect coil 1 to port 1 of network analyzer and connect probe to port 2 of network analyzer.
- 5) Vary coil to phantom distance. Measure S_{11} and S_{21} for each case of coil to phantom distance.

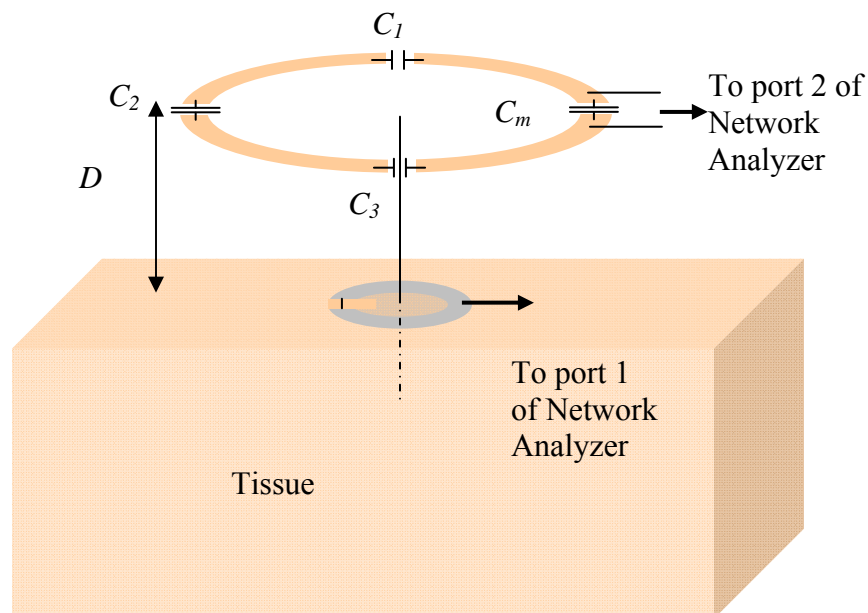


Figure 35 Finding coil to phantom distance for maximizing SNR

Estimate SNR as shown below:

$$\text{Reflected power at port 1 due to mismatch: } P \left(10^{\frac{S_{11}}{10}} \right)$$

$$\text{Net input power to coil 1 at port 1: } P_{in(net)} = P \left(1 - 10^{\frac{S_{11}}{10}} \right)$$

$$\text{Power received by flux probe at port 2: } P_{rec} = P \left(10^{\frac{S_{21}}{10}} \right)$$

$$\text{SNR} = 10 \left[\text{Log}_{10} \left(\frac{P_{rec}}{P_{in(net)}} \right) \right] = 10 \left[\text{Log}_{10} \left(\frac{1 - 10^{\frac{S_{11}}{10}}}{10^{\frac{S_{21}}{10}}} \right) \right]$$

6) Distance for which SNR is maximum would be the desired coil to phantom distance.

2. Finding Distance between Two Next Nearest Elements in Coil Array

- 1) Place both the coils at a distance D from the phantom as shown in Figure 36(a).
- 2) Match and tune the coil for this distance independently.
- 3) Change the overlap distance between two coils. Measure S_{21} for each case.
- 4) Determine overlap distance x between two coils for which S_{21} is minimum.
- 5) Calculate distance between next nearest element (d) as shown in Figure 36(b):

$$d = 2r - 2x \text{ where } r = \text{radius of the coil.}$$

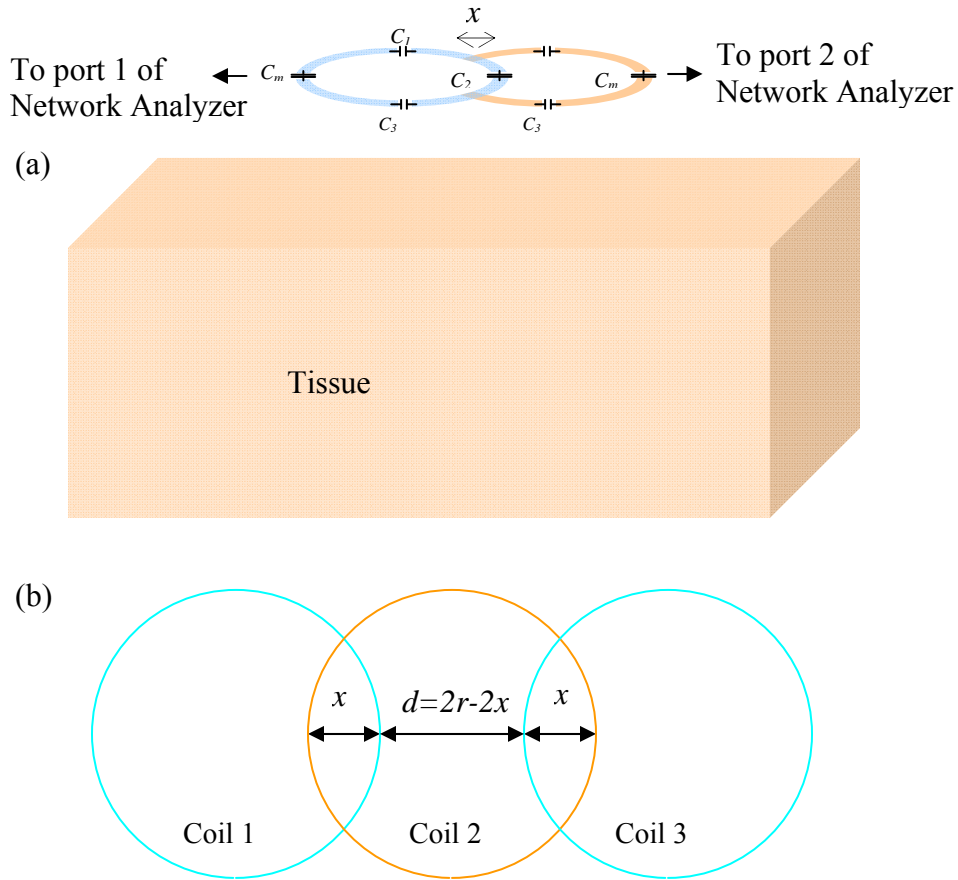


Figure 36 Finding distance between two next nearest elements in the array

3. Method A – Obtaining Equivalent Two Port T-Network

- 1) As shown in Figure 37, remove the preamplifier decoupling network of both the coils (C_m , L and R_p) and measure the impedance of preamplifier decoupling network at coil terminals. Let the impedance be Z_{load} .
- 2) Measure all two port S parameters with port 1 as coil 1 and port 2 as coil 2 terminals.
- 3) Convert S parameters to Z parameters⁴⁸ as follows:

$$Z_{11} = \frac{(1 + S_{11})(1 - S_{22}) + S_{12}S_{21}}{(1 - S_{11})(1 - S_{22}) - S_{12}S_{21}} \quad Z_{12} = \frac{2S_{12}}{(1 - S_{11})(1 - S_{22}) - S_{12}S_{21}}$$

$$Z_{21} = \frac{2S_{21}}{(1-S_{11})(1-S_{22})-S_{12}S_{21}} \quad Z_{22} = \frac{(1-S_{11})(1+S_{22})+S_{12}S_{21}}{(1-S_{11})(1-S_{22})-S_{12}S_{21}}$$

- 4) Obtain two port T circuit comprising of Z parameters⁴⁹ as shown in Figure 38.
- 5) Obtain the current ratio using the following equation:

$$\frac{I_2}{I_1} = \left| \frac{Z_{12}}{Z_{22} + Z_{load}} \right|$$

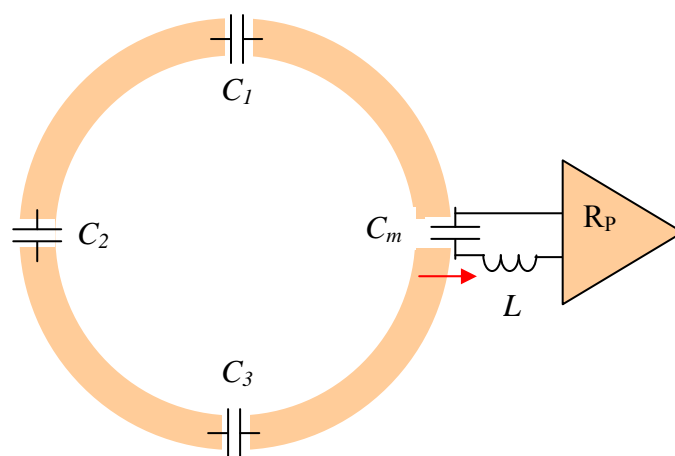


Figure 37 Surface coil with preamplifier decoupling network disconnected

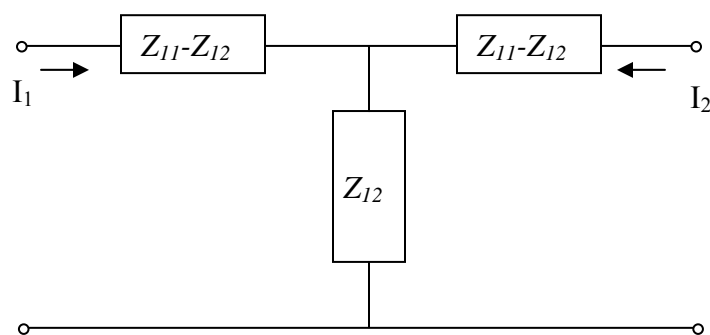


Figure 38 Model of two coil represented as two port T-network with Z parameters

4. Method B – Using Two Flux Probes to Measure Currents in Two Coils

- 1) As shown in Figure 39 connect coil 1 to port 1 of Network Analyzer. Terminate coil 2 with preamplifier for given configuration. Use balun between coil 2 and preamplifier if it is placed at the end of coaxial cable.
- 2) Make two identical flux probes. Probes should be at least a factor of 10 smaller than coil size.
- 3) Place the probe 1 close to coil 1 but away from coil 2. Similarly place the probe 2 close to coil 2 but away from coil 1. Connect both the probes to network analyzer as shown in Figure 39. Use baluns between probes and network analyzer.
- 4) Measure S_{21} and S_{31} parameter in dB.
- 5) Estimate current ratio using the following formula:

$$\frac{I_2}{I_1} = 10^{\left[\frac{S_{31} - S_{21}}{20} \right]}$$

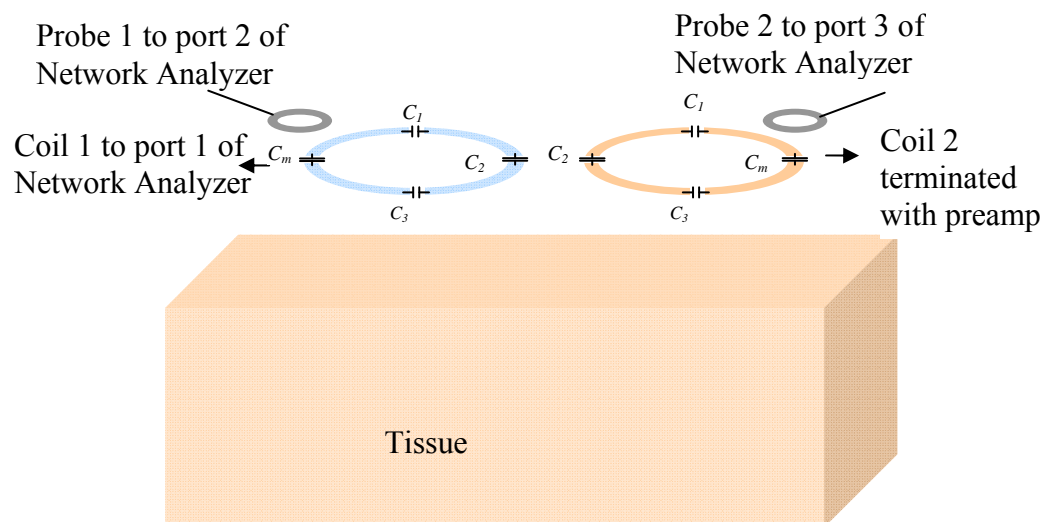


Figure 39 Determining current ratio using two flux probes

B. Metrics for Decision Making

1) Preamplifier Effectiveness

Description: This factor measures how effective a preamplifier is in a given configuration in decoupling two coils

Measurement: I_2/I_1 ratio measurement (Coupling)

Target Value: Better than 0.1.

2) Coil design flexibility

Description: This factor is a measure of complexity in making coil coils with large number of elements on basis of preamplifier placement.

Measurement: Whether preamplifier is placed on the coil or at the end of coaxial cable

3) Preamplifier cost

Description: This factor is a measure of the cost of making the coil on basis of the preamplifier used

Measurement: Knowledge of the type of preamplifier used

Decision Making

- 1) If $I_2/I_1 < 0.1$, it means that coupling is less than -20dB. Isolation of -20dB or better is considered as good isolation between two coils.
- 2) Check if current ratio I_2/I_1 for case A < 0.1 . If it is, use 50Ω standard preamplifier at the end of cable
- 3) Else check if current ratio I_2/I_1 for case B < 0.1 . If it is, use low impedance preamplifier at the end of coaxial.

- 4) Else check if current ratio I_2/I_1 for case C < 0.1 . If it is, place low impedance preamplifier on the coil.
- 5) Else, compare the performance of each configuration.

Suppose $CR_1 = I_2/I_1$ for case A, $CR_2 = I_2/I_1$ for case B and $CR_3 = I_2/I_1$ for case C.

- If $|20\log_{10}(CR_3) - 20\log_{10}(CR_2)| > 2\text{dB}$, there is significant improvement in decoupling by placing the low impedance preamp on the coil. And so, it should be used.
- Otherwise, calculate if $|20\log_{10}(CR_2) - 20\log_{10}(CR_1)| > 2\text{dB}$. If it is, put the preamp away from coil, otherwise 50Ω preamp is good enough, considering the troubles and expenses associated with low input impedance preamp.

C. Decisions for 4.7T Experiment

Table 6 shows that for $d=20\text{mm}$, low impedance preamplifier at the end of coaxial cable had current ratio lesser than 0.0982. Since, it was less than 0.1 it was selected. For $d=15\text{mm}$, the current ratio for low impedance preamplifier at the end of cable (Case B) was above 0.1 while the configuration with low impedance preamplifier at the end of cable had the ratio equal to 0.0742. So, configuration with low impedance preamplifier on the coil was selected.

Table 6 Demonstration of selection of preamp configuration for two cases

Case	Experimental Parameters	Current Ratio (I_2/I_1)			Decision
		Case A	Case B	Case C	
1	$B_0 = 4.7\text{T}; D = 8\text{mm}; d = 20\text{mm}$	0.3573	0.0982	0.0698	Case B
2	$B_0 = 4.7\text{T}; D = 8\text{mm}; d = 15\text{mm}$	0.3894	0.1101	0.0742	Case C

CHAPTER VI

CONCLUSION AND FUTURE WORK

SNR was studied in array of two 3 inch loop coils as a function of preamplifier input impedance, coil loading, intercoil distance and external magnetic field strength. All four methods - Finite Difference Time Domain (FDTD), bench measurement, ADS modeling and image analysis, gave similar results. SNR loss due to coupling is much lower at 3T or higher field strength. Therefore, a coil designer has more flexibility in preamplifier placement at higher field strength. However, preamplifiers should be placed closer to the coils or preferably they should be integrated with the coils to achieve better decoupling and thereby improve SNR.

At lower field strengths, SNR loss is more severe because of significant interaction between coils as a result of poor loading. To preserve SNR, it would be necessary that the preamps be placed on the coil.

Use of standard 50Ω preamplifier was explored by performing coupling measurements at 4.7T. Even at this high field strength, 50Ω preamplifier was ineffective in reducing interaction between two coils. Therefore, the use of low impedance preamplifier is recommended instead of standard preamplifier.

Future work would comprise of developing technology to gather and process data collected by large number of receive channels. Wireless technology should be developed to transmit the signal from coil integrated preamps to the system.

REFERENCES

1. Enderle JD, Bronzino JD, Blanchard SM. Introduction to biomedical engineering. Amsterdam: Elsevier Academic Press; 2005. xxi, 1118 p. p
2. Garach RM. Robust phase sensitive inversion recovery imaging, M.S. Thesis. Texas A&M University at College Station; August 2005.
3. Usey MC. Analysis, design, and application of circularly polarized RF receiver antennas for magnetic resonance imaging, M.S. Thesis. Texas A&M University at College Station; May 1995.
4. Bloch F. 1946. Nuclear induction. *Physical Review*;70(7-8):460.
5. Purcell EM, Pound RV, Bloembergen N. 1946. Nuclear magnetic resonance absorption in hydrogen gas. *Physical Review*;70(11-12):986.
6. Laurterbur PC. 1973. Image formation by induced local interactions: examples employing nuclear magnetic resonance. *Nature*;242(5394):190-191.
7. Damadian R. 1971. Tumor detection by nuclear magnetic resonance. *Science*;171(3976):1151-1153.
8. Mansfield P. 1977. Multi-planar image formation using NMR spin echoes. *J. Phys. C: Solid State Phys.*;10:L55-L58.
9. Frahm J, Haase A, Matthaei D. 1986. Rapid three-dimensional MR imaging using the FLASH technique. *J Comput Assist Tomogr*;10(2):363-8.
10. McDougall MP. Single echo acquisition magnetic resonance imaging, Ph.D Dissertation. Texas A&M University at College Station; December 2006.
11. Brand M, Heid O. 2002. Induction of electric fields due to gradient switching: a numerical approach. *Magn Reson Med*;48(4):731-4.

12. Kimmlingen R, Gebhardt M, Schuster J, Brand M, Schmitt F, Haase A. 2002. Gradient system providing continuously variable field characteristics. *Magn Reson Med*;47(4):800-8.
13. Vogt F, Ladd M, Mateiescu S, Hebrank F, Zhang B, Goehde S. 2002. Impact of increased dB/dT on peripheral nerve stimulation in clinical MRI. *Proc ISMRM*, Honolulu, HI, p 708.
14. Zhang B, Yen YF, Chronik BA, McKinnon GC, Schaefer DJ, Rutt BK. 2003. Peripheral nerve stimulation properties of head and body gradient coils of various sizes. *Magn Reson Med*;50(1):50-8.
15. Boskamp EB. 1987. A new revolution in surface coil technology: the array surface coil. *Proc Soc Magn Reson Med*, New York, p 405.
16. Hyde JS, Jesmanowicz A, Francisz W, Kneeland JB, Grist TM. 1987. Parallel image acquisition for noninteracting local coils. *J Magn Reson*;70:512-517.
17. Requardt H, Tyrell R. 1987. Switched array coils: a new multipurpose tool in MRI. *Proc Soc Magn Reson Med*, New York, p 408.
18. Wright SM, Magin RL, Kelton JR. 1987. Arrays of mutually coupled local coils for high resolution MR imaging. *Proc Soc Magn Reson Med*, New York, p 96.
19. Roemer PB, Edelstein WA, Hayes CE, Souza SP, Mueller OM. 1990. The NMR phased array. *Magn Reson Med*;16(2):192-225.
20. Carlson JW. 1987. An algorithm for NMR imaging reconstruction based on multiple RF receiver coils. *J Magn Reson* 74:376-380.
21. Hutchinson M, Raff U. 1988. Fast MRI data acquisition using multiple detectors. *Magn Reson Med*;6(1):87-91.

22. Kelton JR, Magin RL, Wright SM. 1989. An algorithm for rapid image acquisition using multiple receiver coils. Proc Soc Magn Reson Med. Amsterdam, The Netherlands, p 1172.
23. Kwiat D, Einav S, Navon G. 1991. A decoupled coil detector array for fast image acquisition in magnetic resonance imaging. Med Phys;18(2):251-265.
24. Ra JB, Rim CY. 1993. Fast imaging using subencoding data sets from multiple detectors. Magn Reson Med;30(1):142-5.
25. Wright SM. 2001. Surface coils, arrays and the benefits of array imaging. Workshop on Parallel Imaging. Wurzburg, Germany.
26. Sodickson DK, Griswold MA, Jakob PM. 1999. SMASH imaging. Magn Reson Imaging Clin N Am;7(2):237-54, vii-viii.
27. Sodickson DK, Manning WJ. 1997. Simultaneous acquisition of spatial harmonics (SMASH): fast imaging with radiofrequency coil arrays. Magn Reson Med;38(4):591-603.
28. Pruessmann KP, Weiger M, Scheidegger MB, Boesiger P. 1999. SENSE: sensitivity encoding for fast MRI. Magn Reson Med;42(5):952-62.
29. McDougall MP, Wright SM. 2005. 64-channel array coil for single echo acquisition magnetic resonance imaging. Magn Reson Med;54(2):386-92.
30. Edelman RR. Clinical magnetic resonance imaging. Philadelphia: Saunders Elsevier; 2006. 3 v. (xxiv, 3671, 49, 97 p.) p.
31. Ohliger MA, Ledden P, McKenzie CA, Sodickson DK. 2004. Effects of inductive coupling on parallel MR image reconstructions. Magn Reson Med;52(3):628-39.

32. de Zanche N. 2006. Principles of array system design. Weekday workshop - ISMRM. Seattle.
33. Guclu CC, Boskamp E, Zheng T, Becerra R, Blawat L. 2004. A method for preamplifier-decoupling improvement in quadrature phased-array coils. *J Magn Reson Imaging*;19(2):255-8.
34. Weishaupt D, Köchli VD, Marincek B. How does MRI work? : an introduction to the physics and function of magnetic resonance imaging. Berlin ; New York: Springer; 2003. ix, 138 p. p.
35. Hoult DI, Richards RE. 1976. The signal-to-noise ratio of the nuclear magnetic resonance experiment. *J Magn Reson*;24:71-85.
36. Redpath TW. 1998. Signal-to-noise ratio in MRI. *The British Journal of Radiology*;71:704-707.
37. Boskamp EB. 2004. Transmit and receive RF subsystems. Workshop - ISMRM, Kyoto, Japan.
38. Boskamp EB. 1997. RF coil theory. Unpublished notes, Applied Science Lab, GE Healthcare, Waukesha, WI.
39. Tobgay S. Novel concepts for RF surface coils with integrated receivers, M.S. Thesis. Worcester Polytechnic Institute at Worcester; April 2004.
40. Wright SM, Wald LL. 1997. Theory and application of array coils in MR spectroscopy. *NMR Biomed*;10(8):394-410.
41. Jevtic J. 2001. Ladder networks for capacitive decoupling in phased-array coils. Glasgow, Scotland. p 17:2393.

42. Jevtic J, Pikelja V, Menon A, Seeber D, Tatum N. 2003. Design guidelines for the capacitive decoupling networks. Proc Intl Soc Magn Reson Med. Toronto. p 428.
43. Lee RF, Giaquinto RO, Hardy CJ. 2002. Coupling and decoupling theory and its application to the MRI phased array. Magn Reson Med;48(1):203-13.
44. Reykowski A, Wright SM, Porter JR. 1995. Design of matching networks for low noise preamplifiers. Magn Reson Med;33(6):848-52.
45. Wikipedia. 2007 .http://en.wikipedia.org/wiki/Finite-difference_time-domain_method.
46. Hoult DI. 2000. The principle of reciprocity in signal strength calculations - A mathematical guide. Concepts in Magnetic Resonance;12(4):173-187.
47. Boskamp EB, Feng K, Shah BK, Wright SM. 2007. Array SNR and coupling versus the input impedance of the preamplifier. Proc. ISMRM, Berlin, p 1048.
48. RF Café. 2007. <http://www.rfcafe.com/references/electrical/s-h-y-z.htm>.
49. Stutzman WL, Thiele GA. Antenna theory and design. New York: J. Wiley; 1998. xvi, 648 p. p.

APPENDIX A

Matlab Codes

A1: simulation_results.m

Program that does the following:

- 1) Reads .bfd file and .ssout file if plot requested is Bmag
- 2) Reads .rot.bfd file and .ssout file if plot requested is B+ or B-
- 3) Plots %change in B field per watt dissipated power as a function of intercoil distance
- 4) Plots B field per watt dissipated power as a function of intercoil distance

```

disp('What do you want to plot?');
disp('1) Bmag plot');
disp('2) B+ plot');
disp('3) B- plot');
choice1=input('Enter your choice:');
switch choice1
    case {1}
        disp('You must select .bfd files');
    case {2}
        disp('You must select .rot.bfd files');
    case {3}
        disp('You must select .rot.bfd files');
    otherwise
        disp('Incorrect choice. ');
end
disp('Enter choice of field strength');
disp('1) 3T');
disp('2) 1.5T');
choice2=input('Enter your choice:');
if (choice2 == 1)
    loc=71; start=41; over=132;
elseif (choice2 == 2)
    loc=81; start=52; over=150;
else
    loc=71; start=41; over=132;
end
[x12,y(12,:),Power(12)]=Bfieldplot('Base',loc,start,choice1);
[x1,y(1,:),Power(1)]=Bfieldplot('30mm',loc,start,choice1);
[x2,y(2,:),Power(2)]=Bfieldplot('25mm',loc,start,choice1);
[x3,y(3,:),Power(3)]=Bfieldplot('20mm',loc,start,choice1);
[x4,y(4,:),Power(4)]=Bfieldplot('15mm',loc,start,choice1);
[x5,y(5,:),Power(5)]=Bfieldplot('10mm',loc,start,choice1);
[x6,y(6,:),Power(6)]=Bfieldplot('05mm',loc,start,choice1);
[x7,y(7,:),Power(7)]=Bfieldplot('00mm',loc,start,choice1);
[x8,y(8,:),Power(8)]=Bfieldplot('-05mm',loc,start,choice1);

```

```

[x9,y(9,:),Power(9)]=Bfieldplot('-10mm',loc,start,choice1);
[x10,y(10,:),Power(10)]=Bfieldplot('-15mm',loc,start,choice1);
[x11,y(11,:),Power(11)]=Bfieldplot('-20mm',loc,start,choice1);
p=Power;
x = (0:1.6:over);
s = size(y);
a = s(1); b = s(2);
for i=1:a,
    for j=1:b,
        data2(i,j)=y(i,j)/(sqrt(p(i)));
        j=j+1;
    end
    i=i+1;
end
for i=1:a,
    for j=1:b,
        per_change2(i,j)=(((data2(i,j)-data2(12,j))/data2(12,j))*100); j=j+1;
    end
    i=i+1;
end
new = per_change2(:,1:63);
xnew = x(1:63);

figure(1);
plot(xnew,new(12,:), 'k',xnew,new(1,:), 'y',xnew,new(2,:), 'm',xnew,new(3,:), 'c',xnew,
new(4,:), 'r',xnew,new(5,:), 'g',xnew,new(6,:), 'b',xnew,new(7,:), '-
.k',xnew,new(8,:), '-.b',xnew,new(9,:), '-.g',xnew,new(10,:), '-.r',xnew,new(11,:), '-
.c');
legend('base','30mm','25mm','20mm','15mm','10mm','05mm','00mm','-05mm','-
10mm','-15mm','-20mm');
xlabel('Distance from center of coil 1 along its axis (in mm) --->'); ylabel('%
Change in B Field per Watt dissipated power');
title('Plot 1: Differential plot terminated');

figure(2);
plot(x,per_change2(12,:), 'k',x,per_change2(1,:), 'y',x,per_change2(2,:), 'm',x,per_ch
ange2(3,:), 'c',x,per_change2(4,:), 'r',x,per_change2(5,:), 'g',x,per_change2(6,:), 'b',x,
per_change2(7,:), '-.k',x,per_change2(8,:), '-.b',x,per_change2(9,:), '-
.g',x,per_change2(10,:), '-.r',x,per_change2(11,:), '-.c');
legend('base','30mm','25mm','20mm','15mm','10mm','05mm','00mm','-05mm','-
10mm','-15mm','-20mm');
xlabel('Distance from center of coil 1 along its axis (in mm) --->'); ylabel('%
Change in B Field per Watt dissipated power');
title('Plot 2: Differential plot');

figure(3);

```

```

plot(x,data2(12,:), 'k',x,data2(1,:), 'y',x,data2(2,:), 'm',x,data2(3,:), 'c',x,data2(4,:), 'r',x
,data2(5,:), 'g',x,data2(6,:), 'b',x,data2(7,:), '-.k',x,data2(8,:), '-.b',x,data2(9,:), '-
.g',x,data2(10,:), '-.r',x,data2(11,:), '-.c');
legend('base', '30mm', '25mm', '20mm', '15mm', '10mm', '05mm', '00mm', '-05mm', '-
10mm', '-15mm', '-20mm');
xlabel('Distance from center of coil 1 along its axis (in mm) --->'); ylabel('B Field
per Watt dissipated power (in Tesla)');
title('Plot 3: Bfield per Watt Dissipated Power');

```

```

figure(4);
plot(x,y(12,:), 'k',x,y(1,:), 'y',x,y(2,:), 'm',x,y(3,:), 'c',x,y(4,:), 'r',x,y(5,:), 'g',x,y(6,:), 'b',
x,y(7,:), '-.k',x,y(8,:), '-.b',x,y(9,:), '-.g',x,y(10,:), '-.r',x,y(11,:), '-.c');
legend('base', '30mm', '25mm', '20mm', '15mm', '10mm', '05mm', '00mm', '-05mm', '-
10mm', '-15mm', '-20mm');
xlabel('Distance from center of coil 1 along its axis (in mm) --->'); ylabel('B Field
(in Tesla)');
title('plot 4: Bfield');

```

A.2 Bfieldplot.m

Program that reads .bfd files and .ssout files and returns B field values for all point in the place, B field values for points along axis of coil 1 from its center and dissipated power.

```
function [Bfield,Bplot,Power] =
Bfieldplot(filename,location,startingpoint,choice);
string = strcat('select file : ',filename);
close all; clc;
[fname,pathname]=uigetfile('D:\Bijay Shah\Project 26th\*.*', string);
fullpath=sprintf('%s%s',pathname,fname);
fid=fopen(fullpath,'r');
A = fscanf(fid,'%e');
S=size(A);
Xdim = A(6); Ydim = A(7); Zdim = A(8);
BFD = A(12:S);
BField = reshape(BFD,4,[]);
BFDx = BField(1,:);
BFDy = BField(2,:);
BFDz = BField(3,:);
BFDtotal = BField(4,:);
% Next statement determines whether it is Bmag plot or B+ or B- plot
switch choice
case {1}
    B = reshape(BFDtotal,[],1);
case {2}
    B = reshape(BFDx,[],1);
case {3}
    B = reshape(BFDy,[],1);
otherwise
    % If incorrect choice, plot Bmag
    B = reshape(BFDtotal,[],1);
end
B = reshape(B,Xdim,[]);
Bfplot = B(location,:);
Baxis = Bfplot(startingpoint:Ydim);

Bfield = B;
Bplot=Baxis;
Power = ReadSSOUT(pathname,fname);
```

A.3 ReadSSout.m

Program that reads dissipated power values from .ssout file

```

function DissipatedPower = ReadSSout(PathName,FileName)
DotPos = findstr(FileName, '.');
FileName2 = FileName(1:DotPos);
SSoutFileName = strcat(FileName2, 'ssout');
FullSSoutFileName = strcat(PathName, SSoutFileName);
fpSSout = fopen(FullSSoutFileName);
if(fpSSout == -1)
    disp('Error Opening ssout File');
    return;
else
    disp('SSout File opened successfully');
end
for i = 1:1
    header = textscan(fpSSout, '%s');
    SSoutInfo = header{1};
end
s=size(SSoutInfo);
for i = 1:s(1)
    TF=strcmp('DissipatedPower',SSoutInfo(i));
    if (TF == 1)
        n=i; break;
    end
end
DP = SSoutInfo(n+1);
DissipatedPower = str2num(DP{1});
end

```

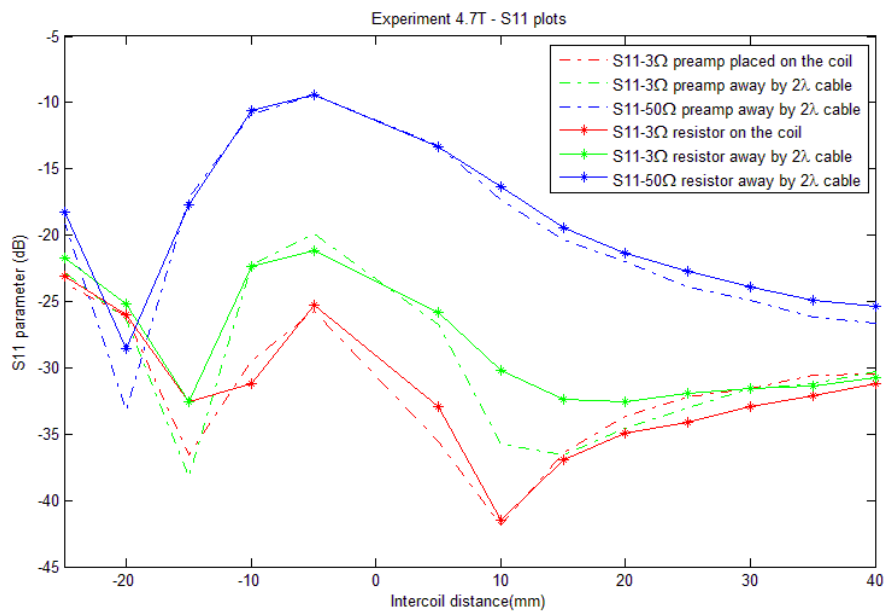
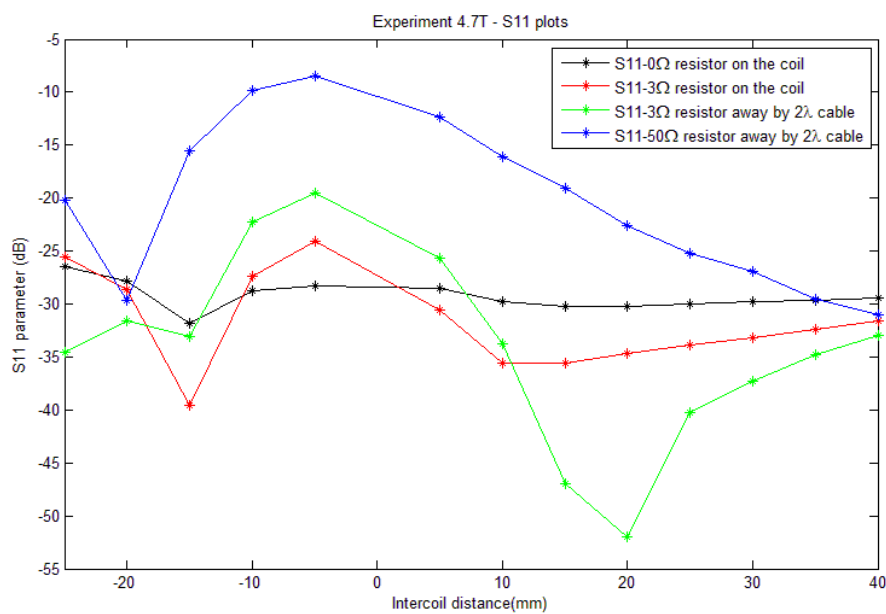
A.4 displayBfield.m

Program that displays B field values obtained from .bfd files.

```
close all; clc; clear all;
[fname,pathname]=uigetfile('D:\Bijay Shah\Project 26th\*.','Select bfd file');
fullpath=sprintf('%s%s',pathname,fname);
fid=fopen(fullpath,'r');
A = fscanf(fid,'%e');
S=size(A);
Xdim = A(6); Ydim = A(7); Zdim = A(8);
BFD = A(12:S);
BField = reshape(BFD,4,[]);
BFDx = BField(1,:);
BFDy = BField(2,:);
BFDz = BField(3,:);
BFDtotal = BField(4,:);
B = reshape(BFDtotal,[],1);
B = reshape(B,Xdim,[]);
figure(1); imagesc(B);
B1 = reshape(BFDtotal,1,[]);
```


APPENDIX B

Plots for Bench Measurements at 4.7T

 S_{11} plotsFigure B1 S_{11} plot for experiment A at 4.7TFigure B2 S_{11} plot for experiment B at 4.7T

S₂₁ Plots

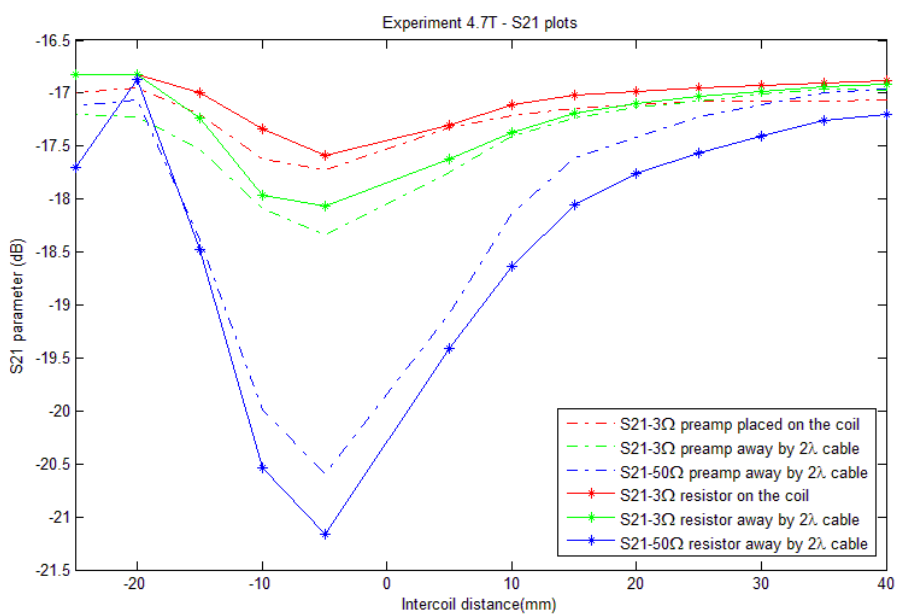


Figure B3 S₂₁ plot for experiment A at 4.7T

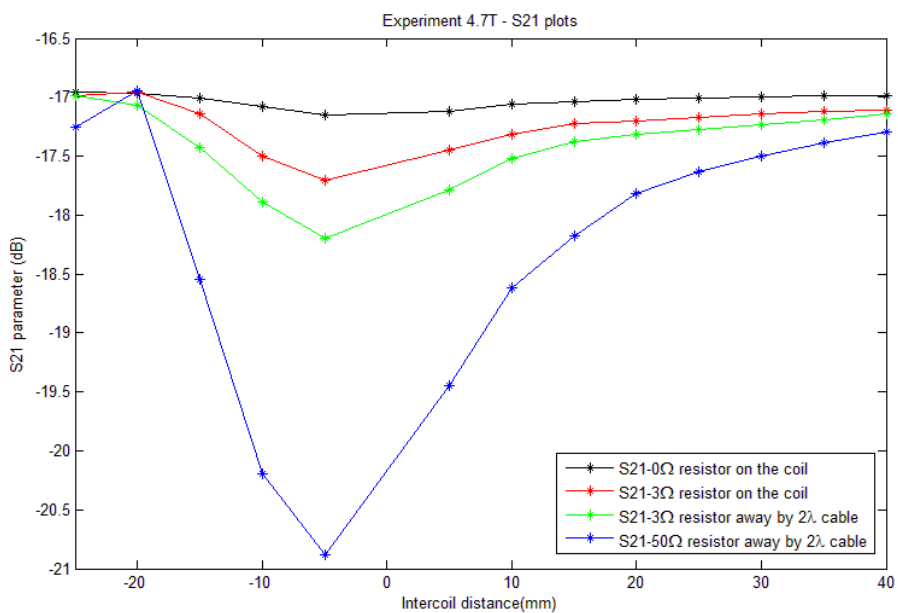
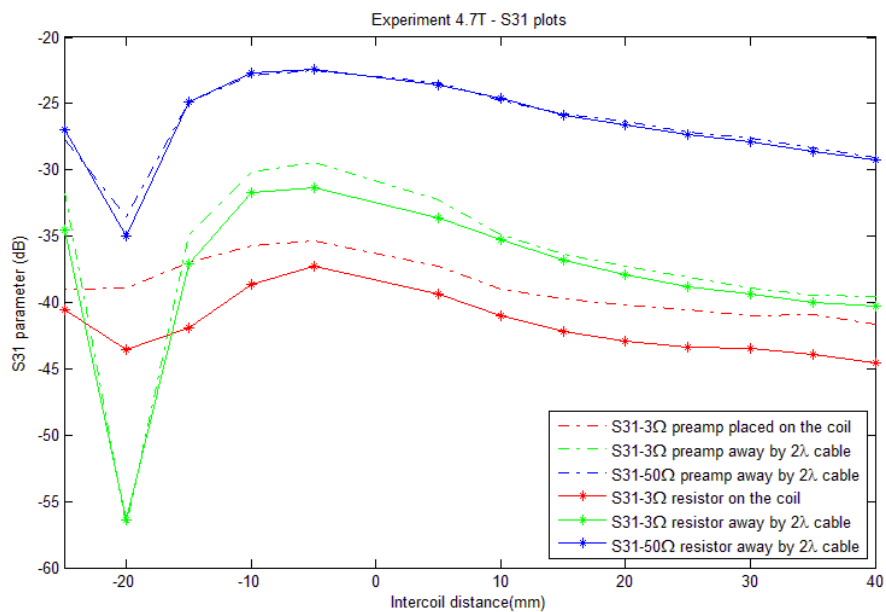
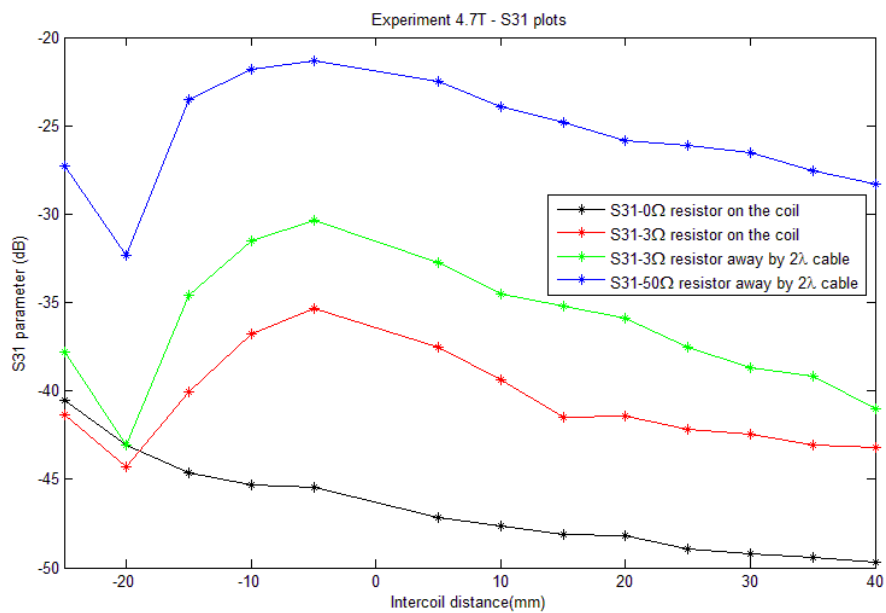


Figure B4 S₂₁ plot for experiment B at 4.7T

S₃₁ PlotsFigure B5 S₃₁ plot for experiment A at 4.7TFigure B6 S₃₁ plot for experiment B at 4.7T

VITA

Bijay Kamleshbhai Shah was born in Surendranagar, Gujarat, India in 1982 to Mr. Kamlesh Shah and Mrs. Rekha Shah. He graduated from Saurashtra University, India in June 2004 with a Bachelor of Engineering degree in biomedical engineering. In 2005, he began his M.S. in biomedical engineering at Texas A&M University. His research area is related to Magnetic Resonance Imaging (MRI). Apart from MRI, he is also interested in exploring other areas of biomedical engineering.

The author can be contacted at his permanent address or email address given below:

A/301, Anal Towers,
Near H. L. Six roads,
Navrangpura,
Ahmedabad-380009
Gujarat, India
Email: shahbijay@gmail.com